Popular Summary

Algorithm Development and Validation for Satellite-Derived Distributions of DOC and CDOM in the U.S. Middle Atlantic Bight

Antonio Mannino[1], Mary E. Russ[1,2], Stanford B. Hooker[1]

[1]NASA Goddard Space Flight Center, Greenbelt, MD, USA
[2]University of Maryland Baltimore County – Goddard Earth Science and Technology

Carbon is the basic building block of life, and the carbon cycle represents the cycle of all living organisms. Through the process of photosynthesis, plants on land or algae living in lakes and oceans take up carbon dioxide and convert this into living organic products (such as carbohydrates, proteins, fats, etc.). Through the process of respiration, organisms break down these organic compounds for energy, metabolizing them into various forms of chemical energy and regenerating the carbon dioxide. The level of carbon dioxide in the atmosphere plays an important role in earth's climate through the "greenhouse effect". Therefore, understanding the carbon cycle provides insight about life on earth as well as its role in climate change. The carbon component of interest here is dissolved organic carbon (DOC), which comprises >97% of the organic carbon in the ocean. The dissolved organic carbon in the coastal ocean originates from many sources, including land plant debris and pollution transported by rivers and material excreted from algae and other living organisms in the ocean. Our objective in this study was to quantify DOC from space through the portion of DOC that can be seen by satellite sensors – colored dissolved organic matter (CDOM). The substance that leaches from tea bags is an example of CDOM. Satellite instruments used to study ocean biology do not measure ocean constituents directly, but rather measure light leaving the ocean at multiple wavelengths (blue, green, red, etc.), which can be used to derive the concentration of ocean constituents, including chlorophyll and CDOM. In fact, the presence of high levels of CDOM in coastal waters reduces the accuracy of satellite chlorophyll measurements.

We conducted multiple expeditions within the coastal ocean region along the U.S. Mid-Atlantic to collect measurements of DOC, CDOM, and light leaving the ocean to develop relationships to compute CDOM and DOC from NASA's MODIS and SeaWiFS satellite sensors. We also evaluated the accuracy of the satellite measurements through comparisons with independent measurements collected at sea. Our results demonstrate that the accuracies of satellite-derived measurements are within 9% for DOC and 20% for CDOM for our coastal ocean study region. These results compare very well with the 33% accuracy for satellite estimates of ocean chlorophyll globally. This study represents the first successful and verified satellite measurements of dissolved organic carbon and colored dissolved organic matter in the coastal ocean. These new satellite products can be applied to study coastal ocean processes such as the export of DOC from land to the ocean, the summer accumulation of DOC from algae and other organisms, and the summer bleaching of CDOM by sunlight. We can apply these satellite observations to investigate interannual and decadal-scale variability in surface ocean CDOM and DOC within coastal waters and monitor impacts of climate change and human activities on coastal ecosystems.

Abstract

In coastal ocean waters, distributions of dissolved organic carbon (DOC) and chromophoric dissolved organic matter (CDOM) vary seasonally and interannually due to multiple source inputs and removal processes. We conducted several oceanographic cruises within the continental margin of the U.S. Middle Atlantic Bight (MAB) to collect field measurements in order to develop algorithms to retrieve CDOM and DOC from NASA's MODIS-Aqua and SeaWiFS satellite sensors. In order to develop empirical algorithms for CDOM and DOC, we correlated the CDOM absorption coefficient (a_{CDOM}) with in situ radiometry (remote sensing reflectance, Rrs, band ratios) and then correlated DOC to Rrs band ratios through the CDOM to DOC relationships. Our validation analyses demonstrate successful retrieval of DOC and CDOM from coastal ocean waters using the MODIS-Aqua and SeaWiFS satellite sensors with mean absolute percent differences from field measurements of <9% for DOC, 20% for $a_{CDOM}(355)$, 16% for $a_{CDOM}(443)$, and 12% for the CDOM spectral slope. To our knowledge, the algorithms presented here represent the first validated algorithms for satellite retrieval of a_{CDOM}, DOC, and CDOM spectral slope in the coastal ocean. The satellite-derived DOC and a_{CDOM} products demonstrate the seasonal net ecosystem production of DOC and photooxidation of CDOM from spring to fall. With accurate satellite retrievals of CDOM and DOC, we will be able to apply satellite observations to investigate interannual and decadal-scale variability in surface CDOM and DOC within continental margins and monitor impacts of climate change and anthropogenic activities on coastal ecosystems.

1. Introduction

The potentially large fluxes of carbon, production, and carbon sequestration in the coastal ocean accentuate the significance of the coastal ocean to the global carbon cycle. Globally, rivers export an estimated but variable 0.43 Pg organic carbon yr^{-1} ($Pg = 10^{15}$ g; Schlünz and Schneider 2000; Ludwig et al. 1996) and 0.4 Pg inorganic carbon yr^{-1} to the ocean (McKee 2003 and references therein). Dissolved organic carbon (DOC) alone comprises over 80-90% of the organic carbon found in the coastal ocean (e.g., Bates and Hansell 1999) and constitutes one of the largest pools of organic carbon in the biosphere (Hedges 2002). The coastal ocean accounts for 21% of the ocean's primary production (Jahnke 2007). The net ecosystem production (NEP) of DOC, which can be generally defined as the sum of phytoplankton extracellular release, lysis of phytoplankton, and zooplankton sloppy feeding and egestion minus microbial uptake, contributes approximately 20% of total primary production in the ocean (Hansell and Carlson 1998; Álvarez-Salgado et al. 2001).

Estuaries and the coastal ocean experience a high degree of variability in the composition and concentration of chromophoric dissolved organic matter (CDOM) and particulate matter as a consequence of the variability in the discharge of terrigenous dissolved organic matter, sediments, and detritus into coastal waters by rivers and estuaries and phytoplankton blooms (Bricaud et al. 1981; Carder et al. 1989; Aiken et al. 1992). This complicates the bio-optical properties of the coastal ocean due to the strong absorptive character of terrigenous CDOM, detritus, and phytoplankton and impedes accurate satellite-based measurements of other ocean color constituents such as chlorophyll a. In coastal waters, CDOM can dominate the inherent

light absorption at ultraviolet and blue wavelengths (20-70% at 440 nm; Del Vecchio and Subramaniam 2004) and confound the retrieval of chlorophyll a from ocean color satellite observations (Bricaud et al. 1981; Nelson and Guarda 1995; Degrandpre et al. 1996). However, the capability to quantify CDOM can lead to improvements in satellite retrievals of chlorophyll a and biogeochemical processes in the coastal ocean. Algorithms developed for the GeoEye/NASA Sea-viewing Wide Field-of-view Sensor (SeaWiFS) (Hoge et al. 2001; Maritorena et al. 2002) and the NASA Moderate Resolution Imaging Spectroradiometer (MODIS) (Carder et al. 1999) estimate the absorption coefficient of CDOM and detritus as a single parameter (a_{CDM}), because CDOM and detritus have similar spectral responses in the visible spectrum.

Several algorithms have been developed to retrieve a_{CDM} from remote sensing of the ocean (Siegel et al. 2002; 2005; Carder et al. 1999), and in the MAB specifically (Hoge et al. 2001; Magnuson et al. 2004). These methods use semi-analytical models to simultaneously derive multiple parameters including a_{CDM}, chlorophyll a, and the particulate backscatter coefficient. Other methods are empirical, relating the CDOM absorption coefficient (a_{CDOM}) to remote sensing reflectance (Rrs) band ratios of various ocean color bands. D'Sa and Miller (2003) found strong relationships between a_{CDOM}(412 nm) and several Rrs band ratios (Rrs; 412 nm/510 nm, 443 nm/510 nm and 510 nm/555 nm) in the Mississippi River plume. At the CalCOFI site in southern California, Kahru and Mitchell (2001) applied the SeaWiFS Rrs(443/510) band ratio to retrieve a_{CDOM}(300). Johannessen et al. (2003) linked ultraviolet (UV) attenuation coefficients (K_d) at 323 nm, 338 nm, and 380 nm to the Rrs(412/555) band ratio ($R^2 > 0.9$), and also found a strong relationship between K_d and a_{CDOM} for each of the UV bands for the coastal ocean adjacent to the Chesapeake and Delaware Bays. By deriving K_d from SeaWiFS normalized water-leaving radiances, Johannessen et al. (2003) retrieved a_{CDOM} to within 6-50% of in situ measurements.

One global approach to estimate DOC from a_{CDM} utilizes a temperature-based algorithm (Siegel et al. 2002). Although this approach has potential for the pelagic ocean, temperature is not likely to be a good indicator of CDOM or DOC in the coastal ocean. Instead, a CDOM-based algorithm that incorporates remote sensing estimates of salinity would seem appropriate, since both DOC and CDOM can co-vary with salinity in coastal waters (e.g., Mantoura and Woodward 1983; Del Vecchio and Blough 2004). At present, however, satellite-based measurements of salinity do not exist and data from planned missions such as the joint NASA-Space Agency of Argentina Aquarius mission will be too coarse (~100km pixels) to be useful in the coastal ocean. The most practical approach to estimate DOC in coastal waters from satellite sensors requires a_{CDOM}- or a_{CDM}-based algorithms. Consequently, we are applying an empirical least-squares approach to estimate DOC from a_{CDOM} by applying relationships derived from field measurements collected within the U.S. Middle Atlantic Bight (MAB). The objectives of this activity were to develop and validate satellite algorithms for retrieval of CDOM and DOC within the MAB.

2. Methods

2.1 Study Area

The focus of this study is on the continental margin of the MAB extending from the Delaware Bay mouth to the region south of the Chesapeake Bay mouth (Fig. 1). The general circulation pattern of the MAB is an along-shore southward flow of shelf water from George's Bank (northeast of the MAB) to Cape Hatteras, North Carolina. During winter and early spring northerly winds and the along-shore current force estuarine plumes, including Chesapeake Bay (Rennie et al. 1999; Verity et al. 2002) and Delaware Bay (Sanders and Garvine 2001) to flow southward along the coast. As winds reverse later in spring the southerly along-shore flow weakens, and the Chesapeake Bay plume broadens and flows offshore, primarily to the south and east. This permits the surface heat flux to strengthen the water column stratification (Verity et al. 2002). At this point, saline waters from the South Atlantic Bight and the Gulf Stream also flow into the southern MAB. A significant portion of shelf water from the MAB is advected offshore from the region between Cape Hatteras and Chesapeake Bay (Churchill and Berger 1998; Verity et al. 2002), which suggests that this region is an important site for carbon export to the open ocean. The drainage basin of Chesapeake Bay discharges more freshwater than any other river along the U.S. Atlantic coast, contributing about half the freshwater that flows into the MAB (Schubel and Pritchard 1986). Freshwater flowing into Delaware Bay contributes ~15-20 % of the freshwater discharge into the MAB (Lebo and Sharp 1993).

2.2 Field sampling

Multiple research cruises were conducted in the southern MAB (Fig. 1) from March 2005 to November 2006 (30 March to 1 April, 27 May, 26-30 July, and 3 November 2005; 9-12 May, 2-6 July, 6 September, and 28 November 2006) to collect biogeochemical (phytoplankton pigments and DOC) and apparent (AOP; water-leaving radiances) and inherent optical properties (CDOM absorption). We also participated on Old Dominion University's hydrography cruises within the lower Chesapeake Bay between July 2004 and September 2005 (5 July, 1 September, 15 October, and 15 November 2004, 10 January, 26 May, 21 June, 19 August, and 23 September 2005; Fig. 1a). Seawater samples were collected with Niskin-type bottles at multiple depths per station. The entire contents of the Niskin bottles were dispensed into carboys, which were shaken prior to sampling to ensure homogeneous samples.

2.3. Sample Collection, Storage, and Analysis

Seawater samples for analysis of DOC and CDOM absorption are filtered under a gentle vacuum (<5 in Hg) through pre-combusted (6 hours at 450°C) Whatman GF/F glass fiber filters and collected directly into pre-cleaned and pre-combusted sample glass bottles and vials. Duplicate samples for DOC analysis are collected and stored frozen. DOC is measured in triplicate (3 of 7 injections to maintain a standard deviation <2%) by high temperature combustion oxidation using a Shimadzu TOC-V instrument (Benner and Strom 1993; Sharp et al. 2002). The deep seawater consensus reference material (CRM; Hansell Laboratory, Rosenstiel School of Marine and Atmospheric Science, University of Miami) is used daily, typically 2 to 3 sets of injections, to verify the accuracy of DOC measurements and maintain an analytical error to within ≤5%. The deep seawater CRM measurements for batch 4 2004 (44.1±1.7 μmol L^{-1} C; n=50) and batch 5 2005 (45.7±1.5 μmol L^{-1} C; n=33) analyzed were within reported consensus values (44-45 μmol L^{-1} C and 45-46 μmol L^{-1} C, respectively).

Standard curves of the manufacturer-recommended carbon standard (potassium hydrogen phthalate) ranging in concentration from 42 to 333 μmol L^{-1} C are conducted prior to analysis each time the catalyst is replaced. Furthermore, standards are interspersed between every 9 samples for each sample batch to verify the consistency of the standard curve throughout each sample batch analyzed. The instrument carbon blank is determined from the area counts of the numerous Milli-Q ultraviolet oxidized ultra-pure water injections and is subtracted from each sample analyzed. To minimize blockage of the TOC-V flow path from salt accumulation, Milli-Q water blanks are inserted between every 3 seawater samples for each batch of samples. Injection volumes for seawater samples, standards and blanks are typically 120 μL.

Samples for determination of CDOM spectral absorption coefficients are stored under refrigeration. In the laboratory, CDOM samples are warmed to room temperature and filtered through 0.2 μm Whatman Nuclepore polycarbonate filters or Gelman Supor (polyethersulfone) filters prior to analysis. Filtration of CDOM samples through GF/F filters in the field is necessary for coastal ocean waters due to the high particle load that quickly clog Nuclepore and Supor filters. Absorbance spectra of CDOM are measured using a Cary 100 Bio Ultraviolet-Visible scanning spectrophotometer and Suprasil quartz 100 mm pathlength cells with ultraviolet (UV) oxidized Milli-Q water as the blank and reference (Mitchell et al. 2003). Instrument scan settings are as follows: 250-800 nm wavelength scan range, 1 nm data interval, 100 nm min^{-1} scan rate, and 4 nm slit width. The instrument noise for reference baselines of air-to-air and ultra-pure water spectral scans is within ±0.0005 absorbance units. Spectral absorption coefficients are determined after subtracting the raw absorption measurements with field filtration blanks of UV-oxidized Milli-Q and a null point value (Mitchell et al. 2000; 2003). For the work presented here, the absorption spectra of filtration blanks and null point value are within the level of instrument noise; thus, additional corrections are not necessary. The absorption coefficients are calculated from the following expression: $a(\lambda)=2.303A(\lambda)/L$, where $A(\lambda)$ is the absorbance of filtered seawater measured across pathlength L in meters. Instrument performance tests (wavelength accuracy and reproducibility, photometric noise, and baseline flatness) are conducted each day prior to analysis. Furthermore, National Institute of Standards and Technology (NIST)-traceable calibration standards (Holmium oxide filter for wavelength accuracy and Spectronics standards, Thermo Electron Corporation, to evaluate stray light, wavelength accuracy, and photometric performance) are also used to verify instrument performance. The uncertainty associated with CDOM spectral absorption coefficients at an instrument noise level of 0.012 m^{-1} is on the order of 0.02-0.046 m^{-1} (Blough and Del Vecchio 2002). The CDOM spectral slope is determined by fitting a single-exponential non-linear curve [$a(\lambda)=a(\lambda_o)e^{-S(\lambda-\lambda_o)}$, where $a(\lambda)$ and $a(\lambda_o)$ represent the absorption coefficients at wavelength λ and reference wavelength λ_o]. CDOM absorption coefficients, $a_{CDOM}(\lambda)$, and the spectral slope coefficient (S), a parameter that quantifies the exponential absorption decrease with increasing wavelength, have been shown to vary with type and source of CDOM (e.g., Blough and Del Vecchio 2002).

Samples for pigment analysis are collected on 25 mm GF/F filters under a gentle vacuum (<5 in Hg). Pigment samples are preserved in liquid nitrogen in the field and stored at -80°C in the laboratory. Pigments are analyzed by reverse-phase high-performance liquid chromatography (HPLC) with a C8 column on the HPLC system equipped with photodiode array detector at the NASA-selected laboratory in support of the NASA MODIS team (currently Horn Point Laboratory, University of Maryland Center for Environmental Science) (Van Heukelem and

Thomas 2001). With this method, uncertainty for total chlorophyll a is 5-7% and 4-15% for carotenoid pigments (Claustre et al. 2004).

2.4 Apparent Optical Properties

The AOP data used here are part of a larger enterprise to create a Self-Consistent AOP Profiles Archive (SCAPA). This database was created from an extensive set of field campaigns executed by a single field team throughout the world ocean (McClain et al. 2004), but primarily in Case-1 waters. The self-consistency of the data products is achieved from a rigorous adherence to The Ocean Optics Protocols (Mueller 2003), with particular emphasis on a set of quality assurance procedures implemented during the sensor calibration, field acquisition, and data processing steps (only the most recent or the most comprehensive references are given): a) the radiometric calibration facilities are traceable to the National Institute of Standards and Technology (NIST) and have all been evaluated in international round robins which showed the absolute calibration uncertainties were to within 3% (Hooker et al. 2002a); b) individual sensor characterizations (e.g., the immersion factor) have been evaluated using standard and new advanced techniques in international round robins and shown to have an uncertainty of less than 1% (Hooker and Zibordi 2005); c) platform perturbations are avoided by using free-fall instruments that can be deployed far away (usually 30-50m) from the deployment platform (Hooker and Morel 2003); d) sensor stability is monitored in the field with a portable source (Hooker and Aiken 1998) or by simultaneous deployment of two or more similar instruments, and the intercomparison of the data products is to within the uncertainty in the calibrations (Hooker et al. 2002b); e) solar irradiance data is collected with a separate sensor mounted on the deployment platform (Hooker and Maritorena 2000), so small illumination variations can be removed from the profile data (the emphasis is on collecting data only during stable atmospheric conditions); f) two-axis tilt sensors are used to ensure only nadir radiances and planar irradiances (to within 5 degrees of vertical) are used during data processing (Hooker and McClain 2000); g) in-water data products are derived from a near-surface extrapolation interval (a portion of the water column that starts close to the sea surface and extends downward for several or many meters as long as the water properties appear homogeneous and the log-transformed data decay linearly) and a well-established methodology (Smith and Baker 1984) that has been evaluated in an international round robin (Hooker et al. 2001) and shown to be capable of agreement at the 1% level; h) because the in-water red wavelengths decay the most rapidly, separate extrapolation intervals are used for the blue-green and red channels, and the choice in setting the deeper limit of the interval (both must have the same shallower limit) is guided by ensuring the extrapolated in-water determination of downward irradiance matches the solar reference (usually to within 2.5% and almost always to within 5%); and i) all the contemporaneous chlorophyll a data, which are needed for some of the processing options (e.g., the self-shading and bidirectional corrections), come from high performance liquid chromatography analysis (Hooker et al. 2005). Although the more recent emphasis has been on collecting data in optically more complex (coastal) waters (Russ et al. 2007), the aforementioned quality assurance procedures are a continuing aspect of these field campaigns. The primary objective is to collect AOP data with an absolute uncertainty less than 5%, so the data can be used for calibration or validation exercises with equal efficacy. One of the most useful data products for such inquiries is the remote sensing reflectance (Rrs), which is a primary variable for deriving satellite algorithms. In situ Rrs observations have successfully been used to quantify chlorophyll a concentrations at remote sensing wavelengths--more properly band ratios (O'Reilly et al. 1998; 2000)--and the intent here

is to establish ocean color algorithms to obtain satellite observations of DOC and CDOM using a similar approach. The spectral configurations of AOP profilers are necessarily tied to the remote sensing and scientific research objectives. The former require a well-defined set of wavelengths, whereas the latter permit a wider diversity of choices. The BioPRO instrument (Biospherical Instruments, Inc.; San Diego, CA) band set is a compromise between these two requirements and is composed of the following wavelengths (each 10nm wide): 320, 340, 380, 395, 412, 443, 465, 490, 510, 532, 555, 560, 625, 665, 670, 683, 710, 780, and 860 nm. Only the AOP data collected on the 2005 research cruises (30 March to 1 April, 27 May, 26-30 July, and 3 November 2005) are applied in the work presented here.

2.5 Algorithm development and validation

In order to develop empirical algorithms for CDOM and DOC, we collected field measurements to correlate a_{CDOM} (CDOM absorption coefficient) to remote sensing reflectance (Rrs) band ratios and then correlated DOC to Rrs band ratios through the a_{CDOM} to DOC relationships. Because CDOM contributes to light absorption across the visible spectrum, several band ratio solutions are possible to avoid the atmospheric correction problems associated with the 412nm band in coastal waters (e.g., negative water-leaving radiances). The least-squares approach was applied to our field observations to evaluate multiple curve-fitting solutions to correlate a_{CDOM} to several Rrs band ratios. The most promising curve-fitting functions, logarithmic and one-phase exponential decay, and Rrs band ratios are presented here. The in situ Rrs value for 551 nm was determined from a linear interpolation of the field measurements of Rrs at 532, 555, and 560 nm. The DOC and a_{CDOM} values were transformed as the inverse of DOC and natural log of $a_{CDOM}(355)$ to meet normality assumptions for model II linear regression analysis. The CDOM spectral slope can also be derived from empirical a_{CDOM} algorithms. Relationships between a_{CDOM} and the Rrs band ratios are derived for multiple a_{CDOM} wavelengths (e.g., from 300 to 469nm) to estimate a_{CDOM} with MODIS and SeaWiFS data at each of those wavelengths. The single exponential non-linear curve fit described previously is applied to the discrete a_{CDOM} values to estimate S.

The validation protocols described by Bailey and Werdell (2006) were applied with the exceptions that the 3x3 ~1km pixel arrays (sensor native resolution) centered on the field station locations were analyzed, rather than 5x5 pixel arrays due to the greater spatial heterogeneity in coastal waters, and the time window between the satellite overpass and field sampling was extended from 3 hours to 8 and 32 hours to provide sufficient validation data points. The percent coefficients of variation within the 3x3 pixel arrays were on average 4.6-6.2% for the relevant SeaWiFS and MODIS Rrs bands (412, 443, 488, 490, 551, and 555 nm), except for the SeaWiFS 412 nm band (14%). SeaWiFS and MODIS-Aqua ocean color observations were processed using SeaDAS versions 4.9.4 and 5.0.5 (msl12 version 5.4.2) and IDL 6.1 or 6.3 from level 1A and/or 1B to level 2 data applying atmospheric corrections and masks for pixels within any of the followings flags (land, cloud or ice, high top-of-atmosphere radiance, low normalized water-leaving radiance at 555 or 551 nm, stray light, sun glint, or atmospheric correction failure) as detailed in Bailey and Werdell (2006). Pixels with water-leaving radiance values <0.2 mW cm^{-2} μm^{-1} sr^{-1} for the 412 nm band were excluded to minimize the impacts of atmospheric correction that may cause negative or reduced water-leaving radiances (Siegel et al. 2002). Validation results presented here exclude all stations where in situ radiometry measurements were applied to derive the satellite sensor algorithms to ensure that the validation dataset is independent from

the dataset used to derive the CDOM algorithms, except where otherwise noted. Multiple band-ratio algorithms were evaluated with the most promising algorithms yielding similar results. The satellite images presented here were derived from the exponential one-phase decay relationship between a_{CDOM} and Rrs(488 nm/551 nm) for MODIS-Aqua and Rrs(490 nm/555 nm) for SeaWiFS.

The evaluation of algorithm performance was based on statistical parameters comparing the satellite-derived measurements of a_{CDOM}, DOC, and CDOM spectral slope with the field measurements, which are referred to here as validation match-ups. The statistical parameters applied include the relative percent difference (results not shown), mean and standard deviation of the absolute percent difference (APD), root mean square error (RMSE), and the R^2 and slope values from linear regression analyses of the validation match-ups for each satellite sensor (Bailey and Werdell 2006; Garcia et al. 2006). In the following equations, C_{alg} and $C_{in\ situ}$ represent the parameters of interest (DOC or a_{CDOM}) for the satellite algorithm and field observations, respectively, and N refers to the sample size.

$$\text{Mean APD (\%)} = [\ \sum |(C_{alg} - C_{in\ situ})| / C_{in\ situ}] * 1/N * 100 \quad (1)$$

$$\text{RMSE} = \text{square-root}\{1/N * \Sigma[(C_{alg} - C_{in\ situ})^2]\} \quad (2)$$

Validation match-ups were conducted for measurements collected within ±8 hours of a satellite overpass and within ±32 hours of a satellite overpass in order to obtain sufficient sample size for analysis. Redundant data (multiple observations from a single satellite sensor for an individual validation station) were excluded based on meeting the validation criteria for atmospheric corrections and masking due to flags (Bailey and Werdell 2006) and minimum time difference between satellite overpass and field sample collection. Excluding stations where in situ radiometry measurements were applied to derive the satellite sensor algorithms reduces sample size significantly (N=8 and 20 for MODIS-Aqua ±8 hour and ±32 hour validation period, respectively, rather than N=14 and 27) and limits this validation dataset to the May 2006 sampling. Therefore, results for the expanded validation dataset that include stations where in situ radiometry measurements were used for algorithm development are also presented to extend the MODIS-Aqua validation into summer and fall and augment the Chesapeake Bay plume dataset, which extends the upper range of DOC and a_{CDOM}. Sample size is substantially greater for SeaWiFS validation match-ups primarily due to masking of MODIS-Aqua pixels caused by flags associated with sun glint and stray light.

3. Results and Discussion

3.1 CDOM to DOC relationships

In coastal ocean waters, distributions of DOC and CDOM vary seasonally and interannually due to multiple source inputs including in situ primary production, contributions from adjacent ocean waters, and terrigenous, anthropogenic, and estuarine-derived organic matter entering the coastal ocean from rivers and bays, and removal processes such as advection, microbial remineralization and photooxidation. CDOM represents only a portion of the total DOC pool, and the non-chromophoric content of DOC varies seasonally and regionally due to diverse inputs and losses. Our results show strong but seasonally variable relationships between

a_{CDOM} and DOC for the southern MAB (Fig. 2; R^2>0.85). Moreover, the seasonal relationships are consistent from year-to-year during our study period (2005-2006). For the shelf region, the a_{CDOM}-DOC slopes for the two seasonal relationships are similar (Figs. 2a-2b), whereas the y-intercepts for the summer relationships are much greater than the fall-winter-spring relationships (Figs. 2a-2b). Furthermore, subsets of these data from the Chesapeake Bay mouth and nearby inner-shelf demonstrate equivalent seasonal relationships (Figs. 2c-2d) to the greater MAB region. In contrast, the summer a_{CDOM} to DOC relationships for the Delaware Bay mouth and nearby plume station differ from the MAB relationship (data not shown). This may be due dissimilarities in source inputs, particularly anthropogenic contributions to Delaware Bay DOM from highly absorbing petroleum hydrocarbons (Mannino and Harvey 1999) and black carbon (Mannino and Harvey 2004). Our results show that at least two seasonal algorithms (fall-winter-spring and summer) are required to retrieve DOC from MODIS and SeaWiFS in the MAB due to seasonal variability in the a_{CDOM} to DOC relationship caused by the accumulation of primarily non-chromophoric DOC from net ecosystem production (NEP) and the concomitant loss of CDOM through sunlight-induced photooxidation between late spring to early fall.

Previous studies in coastal waters also show generally strong correlations between a_{CDOM} and DOC. In the southern Baltic Sea, Ferrari et al. (1996) observed a strong relationship between DOC and $a_{CDOM}(355)$ for April and September cruises (R=0.9 and 0.7, respectively), and a poor correlation for an August cruise. Del Castillo et al. (1999) examined DOC and CDOM absorption within the Orinoco River plume in the Caribbean Sea and found a statistically significant correlation (R=0.88) between DOC and $a_{CDOM}(300)$. Results along a transect from the Delaware Bay mouth to the Sargasso Sea showed a strong correlation between fluorescence and $a_{CDOM}(355)$ and also between fluorescence and DOC concentration (Vodacek et al. 1995; 1997). Rochelle-Newall and Fisher (2002) found a statistically significant relationship between $a_{CDOM}(355)$ and DOC ($P<0.01$, $R^2=0.59$) within Chesapeake Bay. For the MAB, the relationship between DOC and $a_{CDOM}(355)$ in the surface mixed layer was significant ($R^2=0.5$ to 0.75) but seasonally variable from summer to autumn (Del Vecchio and Blough 2004), which is consistent with the results presented here. However, the equations relating DOC and $a_{CDOM}(355)$ in Del Vecchio and Blough (2004; e.g., July 1998: $DOC = 55.6\ a_{CDOM}(355) + 98.3$) are substantially different from our results (Fig. 2). These disparities are likely due to differences in end-member sampling, since the DOC samples from Del Vecchio and Blough (2004) extended from Delaware Bay to Gulf Stream and Sargasso Sea waters, whereas our study emphasized the region between the Chesapeake Bay mouth and the shelf break.

3.2 CDOM and DOC algorithm development and validation

Several non-linear and linear curve-fitting routines model the field observations of a_{CDOM} and Rrs band ratios rather well. The most promising algorithms presented here include the exponential one-phase decay models (Rrs band ratio = $span \bullet e^{-c \bullet a_{CDOM}(355)} + plateau$) and the linear regression models applied to log-transformed data (Fig. 3). Alternative algorithms can also be derived for a_{CDOM} at other wavelengths.

SeaWiFS- and MODIS-Aqua-derived estimates of a_{CDOM} and DOC were compared with field observations to determine which algorithms performed best (Figs. 4-5). The absolute percent difference (APD) and root mean square error (RMSE) for SeaWiFS (Fig. 4) and MODIS-Aqua (Fig. 5) a_{CDOM} and DOC products demonstrate similarly good results for most of the algorithms.

Nevertheless, the algorithms based on the Rrs(412/555) band ratio performed poorly in the SeaWiFS validation compared to the other band ratios. The exponential one-phase decay algorithms with the Rrs(488/551) and Rrs(490/555) band ratios were selected based on the results shown and relative consistency in band ratios for the satellite sensors. The mean APD between the satellite sensor and field measurements are approximately 20±20% for $a_{CDOM}(355)$ (mean±1 standard deviation), 16±16% for $a_{CDOM}(443)$ and <8±5% for DOC (Figs. 4-5). Furthermore, expanding the validation dataset to include stations where in situ radiometry measurements were used for algorithm development yields equivalent mean APD values for $a_{CDOM}(355)$ and $a_{CDOM}(443)$, but higher values for DOC (7.3±7.5% and 10.5±7.3% for MODIS-Aqua ±8 hour and ±32 hour overpass periods and 8.5±7.5% and 7.1±6.2% for SeaWiFS ±8 hour and ±32 hour overpass periods). The equations and coefficients for the validated a_{CDOM} and DOC algorithms are described in Tables 1 and 2, respectively.

The validation match-ups of satellite-derived $a_{CDOM}(355)$, $a_{CDOM}(412)$ and $a_{CDOM}(443)$ for these algorithms with the field observations demonstrate a close correspondence to the one-to-one relationship for both SeaWiFS and MODIS-Aqua (Fig. 6). For $a_{CDOM}(355)$ and $a_{CDOM}(412)$, the SeaWiFS match-ups (R^2=0.89 to 0.93; slope=0.73 to 0.83;) are stronger than for MODIS-Aqua (R^2=0.87 to 0.95; slope=0.63 to 0.65) and vice versa for $a_{CDOM}(443)$ (Fig. 6). If the validation match-up dataset is expanded to include stations where in situ radiometry measurements were used for algorithm development then the match-up results improve for SeaWiFS ($a_{CDOM}(355)$: slope=0.93 to 0.97) but deteriorate for MODIS ($a_{CDOM}(355)$: slope=0.52 to 0.545) (Fig. 7). The slope values from the one-to-one validation linear regression analyses may not represent the most informative measure of algorithm performance given the small size of the validation dataset and the relatively narrow range of a_{CDOM} values (about one order of magnitude). The expanded dataset includes more stations within the Chesapeake Bay plume region (primarily from 27 May and 3 November 2005) that may accentuate discrepancies in time and space between water masses observed by the satellite sensor and sample collection from the ship as well as differences in Rrs between the in situ radiometry (490 nm and 555 nm) and the MODIS sensor (488 nm and interpolated 551 nm) because of the more optically complex waters (higher chlorophyll a, suspended particles, and CDOM). Nevertheless, the mean absolute percent differences (APD) for $a_{CDOM}(355)$, $a_{CDOM}(412)$ and $a_{CDOM}(443)$ are essentially equivalent for the independent validation and expanded datasets for both sensors. Furthermore, the vertical heterogeneity in river and estuary outflow regions complicates the comparison of the satellite-derived product and the field measurement selected to represent that particular pixel in the validation match-up. Surface mixed layers were typically one to several meters in depth within the plume regions of Chesapeake Bay and Delaware Bay, and Niskin-type sampling bottles homogenized 0.5 to 1 m layer of the water column. The approach applied here entailed using measurements from the top 2 depths of the water column sampled, typically 0.5 to 2 m and 2.5 to 5 m, and weighting the top depth two times the weight of the second depth. The measurements for the top 2 depths were equivalent for most of the stations sampled. The validation match-ups demonstrate excellent retrieval of CDOM with mean APD values for $a_{CDOM}(355)$ ranging from 14.8±11.7% for SeaWiFS to 21±19.7% for MODIS (Figs. 4-5). For $a_{CDOM}(443)$, the APD range from 12.7±10.3% for SeaWiFS to 16.1±14.6% for MODIS (Figs. 4-5). These values are quite good in comparison to typical satellite retrievals of chlorophyll a globally (33.1% median percent difference; Bailey and Werdell 2006) and retrievals of $a_{CDM}(443)$ (25%; Magnuson et al. 2004) and $a_{CDOM}(350)$ (6-50%; Johannessen et al. 2003) for our study region.

The DOC validation match-ups also show excellent agreement between satellite and field observations (R^2=0.75 to 0.96; Fig. 8). Given the narrow range of DOC concentrations (72 to 162 μM DOC) and limited sample size, the slope from the one-to-one linear regression analyses (0.49 to 0.83; Fig. 8) is not a useful parameter to evaluate algorithm performance. The APD for DOC match-ups demonstrate exceptional equivalence between satellite sensor and field measurements with mean APD values ranging from 3.6±2.2% to 7.6±5.3% for MODIS ±8 hour and ±32 hour satellite overpass period, respectively, and 6.5±5.2% for SeaWiFS (Figs. 4-5). The RMSE values range from 8.2 to 8.6 μM DOC for SeaWiFS and 3.2 to 7.8 μM DOC for MODIS-Aqua. Higher mean APD (10.5±7.3% for MODIS-Aqua and 8.5±7.5% for SeaWiFS) and RMSE values (Fig. 8C) were computed for the expanded dataset, which includes additional stations from summer and fall cruises and from the Chesapeake Bay plume region. This study represents the first validated algorithms for retrieval of surface ocean DOC from SeaWiFS and MODIS satellite sensors. The approach described by Siegel et al. (2002) to determine surface DOC using sea-surface temperatures was successful for entire ocean basins, but is not appropriate for coastal ocean waters just as CDOM- or CDM-based algorithms are not appropriate for the open ocean because of the poor and sometimes negative correlation between a_{CDOM} and DOC in the open ocean.

Exponential one-phase decay Rrs band ratio models were computed for multiple a_{CDOM} wavelengths to develop an algorithm to retrieve the CDOM spectral slope (S). The mean APD for $a_{CDOM}(\lambda)$ used to derive S range from 14±13% to 25±27% (Figs. 9a-9b). The validation results suggest that the CDOM spectral slope can be retrieved from MODIS-Aqua and SeaWiFS to within 12.4±1.7% and 8.7±5.1%, respectively (Figs. 9c-9d). The one-to-one match-ups for S suggest that the MODIS-Aqua product is biased slightly on the high side compared to field observations (Figs. 9e-9f). The relatively narrow range of S observed in the MAB requires particularly accurate satellite retrievals (<10±5%) to apply this product in tracking sources of terrigenous or marine CDOM and quantifying photooxidation of CDOM and DOC. The validation results suggest that the CDOM spectral slope algorithms can be useful for these applications.

3.3 Seasonal variability of $a_{CDOM}(355)$ and DOC

The satellite-derived products reveal strong seasonal variability in CDOM for the continental margin of the MAB. The gradient of high to low a_{CDOM} from the coast to the open ocean is consistent with our field measurements and previous work (Fig. 10; Nelson and Guarda 1995; DeGrandpre et al. 1996; Del Vecchio and Blough 2004). Higher levels of a_{CDOM} along the coast coincide with periods of elevated freshwater outflow from the Chesapeake Bay, Susquehanna River, and Delaware River, particularly during winter-spring (Figs. 10-11; March to May 2005; November to December 2005 and February 2006). Substantial decreases in $a_{CDOM}(355)$ occur from spring to summer, particularly on the mid-shelf, outer-shelf, and continental slope, primarily due to sunlight-induced photooxidation (Vodacek et al. 1997; Fig. 10). During autumn, storm events vertically mix the water column and introduce CDOM-enriched bottom waters to the surface (Fig. 10D). Seasonal vertical stratification isolates DOM at depth from sunlight, which can degrade CDOM, resulting in DOM with greater chromophoric content at depth than at the surface (Vodacek et al. 1997; Nelson and Siegel 2002). Degraded terrestrial vegetation transported by rivers and estuaries appears to be the principal source of CDOM to the

continental margin (Del Vecchio and Blough 2004). Biological processes such as grazing and microbial activity may also contribute a_{CDOM} to the continental margin (Nelson et al. 2002; Steinberg et al. 2004). Hernes and Benner (2003) found a strong correlation between dissolved lignin phenols (compounds derived from vascular plants) and $a_{CDOM}(350)$ within the Mississippi River plume. Such studies demonstrate that a_{CDOM} may be useful as a tracer of terrigenous DOM in the coastal ocean. However, Chen et al. (2002) observed significant inputs of fluorescent CDOM to the MAB from shelf-slope exchange and from upwelling of slope water in Georges Bank and concluded that rivers/estuaries contribute no more than 10% of CDOM fluorescence. Satellite data analysis of surface ocean CDOM and sea-surface temperatures within the MAB may resolve these contrasting results.

The DOC distributions derived from satellite data analysis also reveal significant seasonal variability for the continental margin of the MAB (Fig. 12). As observed for CDOM, DOC concentrations are generally higher along the coast, especially within the outflow regions of Chesapeake Bay and Delaware Bay, during and following periods of high freshwater discharge (April 2005, February 2006, June 2006 and November 2006; Figs. 11-12) and decrease offshore. Much higher DOC concentrations are observed during the summer compared to early spring due to net ecosystem production (NEP) that promotes the accumulation of semi-labile DOC (Fig. 12). The seasonal accumulation of significant quantities of semi-labile DOC typically begins near the end of phytoplankton blooms when nutrients become limiting which promote the excess production of organic carbon by phytoplankton (Williams 1995; Avril 2002; Cauwet et al. 2002; Nieto-Cid et al. 2004). DOC concentrations from several discrete MODIS-Aqua images were averaged across the study region (36-39°N, 74-77°W; as shown in Fig. 11) based on bathymetry (Fig. 13) using the 1km SRTM30_Plus bathymetry data from Becker and Sandwell (2004) for comparison with field measurements. The satellite-derived DOC values for 2005 and 2006 (Figs. 13a-13b) are equivalent to our field measurements (Fig. 13c). Noteworthy differences (~13 μmol C L^{-1}) include the outer shelf and continental slope regions in 2006 (Fig. 13), which can be attributed at least in part to our limited field sampling within those bathymetry regions. The seasonal increases in DOC concentration estimated from the discrete MODIS-Aqua images and field measurements are similar for 2005 and 2006 and range from 22-34 μmol C L^{-1} on the inner shelf (10-20 m), 18-22 μmol C L^{-1} on the mid-shelf (20-60 m), 6-20 μmol C L^{-1} on the outer shelf (60-80 m), and 2-14 μmol C L^{-1} on the continental slope (80-500 m) (Fig. 13). The field measurements reveal a higher seasonal DOC increase on the mid-shelf of 31 and 24 μmol C L^{-1} for 2005 and 2006, respectively, than observed from the MODIS images. The seasonal DOC increase that we computed is consistent with previous field measurements collected by Vlahos et al. (2002) between March and August 1996 within the southern MAB (35 and 21 μmol C L^{-1} within the mid-shelf and continental slope region, respectively). From late autumn through early spring, the water column on the continental shelf is vertically well-mixed to 100 m, thus satellite retrievals of surface ocean products are representative of the entire water column. Field measurements of DOC and a_{CDOM} from March 2005 and May 2006 confirm this. Applying MODIS-Aqua and SeaWiFS observations of surface ocean DOC and the high-resolution bathymetry data (Becker and Sandwell 2004) yielded an estimate of the DOC reservoir of 1.1×10^{12} g C for the southern MAB (10-100 m bathymetry; 36° to 39°N; 77° to 74°W) during the winters of 2005 and 2006. Given accurate mixed-layer depths, the DOC reservoir and NEP of DOC can be estimated within the surface mixed-layer from satellite observations during stratified conditions.

4. Conclusions

Our validation analyses demonstrate successful retrieval of DOC and CDOM from coastal ocean waters using the MODIS-Aqua and SeaWiFS satellite sensors with mean APD from field measurements of <9% for DOC, 20% for $a_{CDOM}(355)$, 16% for $a_{CDOM}(443)$, and 12% for the CDOM spectral slope. The results demonstrate slightly better retrievals of a_{CDOM} products with SeaWiFS than MODIS-Aqua, but equivalent retrievals for DOC and S. To our knowledge, this study contributes the first validated algorithms for satellite retrieval of coastal ocean surface DOC, a_{CDOM}, and CDOM spectral slope. The seasonal processes that influence CDOM distributions in the MAB include freshwater discharge (especially in winter and early spring), photooxidation in summer, and wind-induced vertical mixing of the water column in autumn. DOC distributions are driven primarily by freshwater discharge, net ecosystem production, and the ocean circulation pattern along the shelf and continental slope. Our a_{CDOM} satellite algorithms can be applied beyond this study region if the appropriate field datasets are available to extend the range of the exponential decay model (Fig. 3A) and to validate the a_{CDOM} satellite products. The variability in the a_{CDOM} to DOC relationship limits the application of the specific DOC algorithms presented here to the continental shelf and slope area of the MAB. Nevertheless, the approach presented here is valid for other coastal ocean regions where DOC is strongly correlated to a_{CDOM}. The potential applications for satellite-derived CDOM and DOC products are substantial. Satellite analysis of a_{CDOM} can be used to quantify photooxidation rates (CDOM and DOC loss and inorganic carbon production), track the inputs of terrigenous organic matter from rivers or estuaries into the coastal ocean and beyond, and trace water masses with different CDOM signatures. Satellite-derived DOC can be applied to carbon cycle studies to quantify the fluxes of DOC entering the coastal ocean and exported from the continental margin to the open ocean, estimate DOC produced through NEP, and assess the standing stock of DOC. With accurate satellite retrievals of a_{CDOM} and DOC, we will be able to apply satellite observations to investigate interannual and decadal-scale variability in surface CDOM and DOC within continental margins and evaluate how climate change and anthropogenic activities impact coastal ecosystems.

Acknowledgments

This work was supported by the NASA Ocean Biology and Biogeochemistry Program with grants from the NASA New Investigator Program, Interdisciplinary Science, and Earth Observing System programs. Ship time for July 2005, May and July 2006 was funded by a NOAA grant in support of the Coastal Observatories program. We thank the Captains and crews of the R/V Cape Henlopen, R/V Hugh R. Sharp, and R/V Fay Slover. We are grateful to H. Throckmorton, P. Bernhardt, K.C. Filippino, and M. Linksweiler for help with particle filtration. Special thanks to J. Morrow, J. Brown, D. D'Alimonte and J.-N. Druon for assistance with deploying thee profiling radiometer, L. Van Heukelem and C. Thomas (Horn Point Laboratory) for the HPLC pigment results, and the Ocean Biology Processing Group (OBPG) at GSFC. J. O'Reilly kindly provided the high-resolution bathymetry data.

References

Aiken J., G.F. Moore and P.M. Holligan. 1992. Remote sensing of oceanic biology in relation to global climate change. J. of Phycology 28: 549-590.

Álvarez-Salgado, X.A., J. Gago, B.M. Míguez and F.F. Pérez. 2001. Net ecosystem production of dissolved organic carbon in a coastal upwelling system: the Ría de Vigo, Iberian margin of the North Atlantic. Limnol. Oceanogr. 46: 135-147.

Bates, N.R., and D.A. Hansell. 1999. A high resolution study of surface layer hydrographic and biogeochemical properties between Chesapeake Bay and Bermuda. Mar. Chem. 67: 1-16.

Bailey, S. W. and P. J. Werdell. 2006. A multi-sensor approach for the on-orbit validation of ocean color satellite data products. Remote Sensing of Environ. 102: 12–23.

Becker, J.J. and D.T. Sandwell. 2004. SRTM30_PLUS: Data fusion of SRTM Land Topography with Measured and Estimated Seafloor Topography. Scripps Inst. Oceanography, Univ. California San Diego, 9500 Gilman Drive, La Jolla, CA.

Benner, R. and M. Strom. 1993. A critical evaluation of the analytical blank associated with DOC measurements by high-temperature catalytic oxidation. Mar. Chem. 41: 153-60.

Blough, N.V. and R. Del Vecchio. 2002. Chromophoric DOM in the coastal environment, pp. 509-546. In: Hansell D.A. and Carlson C.A. (eds), Biogeochemistry of Marine Dissolved Organic Matter. Academic Press.

Bricaud, A., A. Morel and L. Prieur. 1981. Absorption by dissolved organic matter of the sea (yellow substance) in the UV and visible domains. Limnol. Oceanogr. 26: 43-53.

Carder, K.L., R.G. Steward, G.R. Harvey and P.B. Ortner. 1989. Marine humic and fulvic acids: their effects on remote sensing of ocean chlorophyll. Limnol. Oceanogr. 34: 68-81.

Carder, K.L., F.R. Chen, Z.P. Lee, S.K. Hawes and D. Kamykowski. 1999. Semianalytic Moderate-Resolution Imaging Spectrometer algorithms for chlorophyll and absorption with bio-optical domains based on nitrate-depletion temperatures. J. Geophys. Res. Vol. 104(C3): 5403-5421 (1998JC900082).

Chen, R.F., Y. Zhang, P. Vlahos and S.M. Rudnick. 2002. The fluorescence of dissolved organic matter in the Mid-Atlantic Bight. Deep-Sea Res. II. 49: 4439-4459.

Churchill, J.H. and T.J. Berger. 1998. Transport of Middle Atlantic Bight shelf water to the Gulf Stream near Cape Hatteras. J. Geophys. Res. 103(C13): 30,605-30,621.

Cauwet, G., G. Déliat, A. Krastev, G. Shtereva, S. Becquevort, C. Lancelot, A. Momzikoff, A. Saliot, A. Cociasu and L. Popa. 2002. Seasonal DOC accumulation in the Black Sea: a regional explanation for a general mechanism. Mar. Chem. 79: 193-205.

Claustre, H., S.B. Hooker, L. Van Heukelem, J.F. Berthon, R. Barlow, J. Ras, H. Sessions, C. Targa, C.S. Thomas, D. van der Linde, J.C. Marty. 2004. An intercomparison of HPLC phytoplankton pigment methods using in situ samples: application to remote sensing and database activities. Mar. Chem. 85: 41-61.

DeGrandpre, M.D., A. Vodacek, R.K. Nelson, E.J. Bruce and N.V. Blough. 1996. Seasonal seawater optical properties of the U.S. Middle Atlantic Bight. J. Geophys. Res. 101: 22,727-22,736.

Del Castillo, C.E., P.G. Coble, J.M. Morell, J.M. Lopez and J.E. Corredor. 1999. Analysis of the optical properties of the Orinoco River plume by absorption and fluorescence spectroscopy. Mar. Chem. 66: 35-51.

Del Vecchio, R., and N.V. Blough. 2004. Spatial and seasonal distribution of chromophoric dissolved organic matter (CDOM) and dissolved organic carbon (DOC) in the Middle Atlantic Bight. Mar. Chem. 89: 169-187.

Del Vecchio, R., and A. Subramaniam. 2004. Influence of the Amazon River on the surface optical properties of the western tropical North Atlantic Ocean. J. Geophys. Res. 109 (C11001), doi:10.1029/2004JC002503.

D'Sa E.J. and R.L. Miller. 2003. Bio-optical properties in waters influenced by the Mississippi River during low flow conditions. Remote Sensing of Eviron. 84: 538-549.

Garcia, V.M.T., S. Signorini, C.A.E. Garcia and C.R. McClain. 2006. Empirical and semi-analytical chlorophyll algorithms in the south-western Atlantic coastal region (25-40°S and 60-45°W). Int. J. Remote Sensing 27: 1539-1562.

Hansell, D.A., and C.A. Carlson. 1998. Net community production of dissolved organic carbon. Global Biogeochemical Cycles 12: 443-453.

Hedges, J.I.. 2002. Why dissolved organic matter, pp. 1-33. In: Hansell D.A. and Carlson C.A. (eds),
Biogeochemistry of Marine Diolved Organic Matter. Academic Press.

Hernes, P.J., and R. Benner. 2003. Photochemical and microbial degradation of dissolved lignin phenols: Implications for the fate of terrigenous dissolved organic matter in marine environments. J. Geophys. Res. 108(C9), 3291, doi:10.1029/2002JC001421.

Hoge, F.E., C.W. Wright, P.E. Lyon, R.N. Swift and J.K. Yungel. 2001. Inherent optical properties imagery of the western North Atlantic Ocean: Horizontal spatial variability of the upper mixed layer. J. Geophys. Res. 106, No. C12 , 31,129-31,138.

Hooker, S.B., and J. Aiken, 1998: Calibration evaluation and radiometric testing of field radiometers with the SeaWiFS Quality Monitor (SQM). J. Atmos. Oceanic Technol., 15, 995-1,007.

Hooker, S.B., and S. Maritorena, 2000: An evaluation of oceanographic radiometers and deployment methodologies. J. Atmos. Oceanic Technol., 17, 811-830.

Hooker, S.B., and C.R. McClain, 2000: The calibration and validation of SeaWiFS data. Prog. Oceanogr., 45, 427-465.

Hooker, S.B., G. Zibordi, J-F. Berthon, D. D'Alimonte, S. Maritorena, S. McLean, and J. Sildam, 2001: Results of the Second SeaWiFS Data Analysis Round Robin, March 2000 (DARR-00). NASA Tech. Memo. 2001-206892, Vol. 15, S.B. Hooker and E.R. Firestone, Eds., NASA Goddard Space Flight Center, Greenbelt, Maryland, 71pp.

Hooker, S.B., S. McLean, J. Sherman, M. Small, G. Lazin, G. Zibordi, and J.W. Brown, 2002a: The Seventh SeaWiFS Intercalibration Round-Robin Experiment (SIRREX-7), March 1999. NASA Tech. Memo. 2002-206892, Vol. 17, S.B. Hooker and E.R. Firestone, Eds., NASA Goddard Space Flight Center, Greenbelt, Maryland, 69pp.

Hooker, S.B., G. Lazin, G. Zibordi, and S. McLean, 2002b: An evaluation of above- and in-water methods for determining water-leaving radiances. J. Atmos. Oceanic Technol., 19, 486-515.

Hooker, S.B., L. Van Heukelem, C.S. Thomas, H. Claustre, J. Ras, L. Schl¸ter, J. Perl, C. Trees, V. Stuart, E. Head, R. Barlow, H. Sessions, L. Clementson, J. Fishwick, C. Llewellyn, and J. Aiken, 2005: The Second SeaWiFS HPLC Analysis Round-Robin Experiment (SeaHARRE-2). NASA Tech. Memo. 2005-212785, NASA Goddard Space Flight Center, Greenbelt, Maryland, 112pp.

Hooker, S.B., and G. Zibordi, 2005: Advanced methods for characterizing the immersion factor of irradiance sensors. J. Atmos. Oceanic Technol., 22, 757-770.

Jahnke, R.A. (2007, in press) *Global Synthesis in Carbon and Nutrient Fluxes in Continental Margins: A Global Synthesis*, K.K. Liu, L. Atkinson, R. Quinones and L. Talaue-McManus, ed. Global Change: The IGBP Series, Springer-Verlag.

Johannessen, S.C., W.L. Miller and J.J. Cullen. 2003. Calculation of UV attenuation and colored dissolved organic mater absorption spectra from measurements of ocean color. J. Geophys. Res. 108(C9), 3301-3313.

Johnson, D.R., J. Miller and O. Schofield. 2003. Dynamics and optics of the Hudson River outflow plume. J. Geophys. Res. 108(C10), 3323, doi:10.1029/2002JC001485.

Kahru, M. and B.G. Mitchell. 2001. Seasonal and nonseasonal variability of satellite-derived chlorophyll and colored dissolved organic matter concentration in the California current. J. Geoophys. Res. 106: 2517-2529.

Lebo, M.E., and J.H. Sharp. 1993. Phosphorus distributions along the Delaware: An urbanized coastal plain estuary. Estuaries 16: 291-302.

Ludwig, W., J.-L. Probst and S. Kempe. 1996. Predicting the oceanic input of organic carbon by continental erosion. Global Biogeochemical Cycles 10: 23-41.

Magnuson, A., L.W. Harding, Jr., M.E. Mallonee, and J.E. Adolf. 2004. Bio-optical model for Chesapeake Bay and Middle Atlantic Bight. Estuar. Coast. Shelf Sci. 61: 403-424.

Mannino, A. and H.R. Harvey. 1999. Lipid composition in particulate and dissolved organic matter in the Delaware Estuary: sources and diagenetic patterns. Geochimica et Cosmochimica Acta, 63: 2219-2235, 1999.

Mannino, A. and H.R. Harvey. 2004. Black carbon in estuarine and coastal ocean dissolved organic matter. Limnol. & Oceanogr. 49: 735-740.

Mantoura, R.F.C. and E.M.S. Woodward. 1983. Conservative behavior of riverine dissolved organic carbon in the Severn estuary: chemical and geochemical implications. Geochimica et Cosmochimica Acta 47, 1293-1309.

Maritorena, S., D.A. Siegel, A.R. Peterson. 2002. Optimization of a semianalytical ocean color model for global-scale applications. Appl. Opt. 41: 2705-2714.

McClain, C.R., G.C. Feldman, and S.B. Hooker, 2004: An overview of the SeaWiFS project and strategies for producing a climate research quality global ocean bio-optical time series. Deep Sea Res. II, 51, 5-42.

McKee, B.A. 2003. RiOMar: The Transport, Transformation and Fate of Carbon in River-dominated Ocean Margins. Report of the RiOMar Workshop, 1-3 November 2001. Tulane University, New Orleans, LA.

Mitchell, B.G., et al. 2000. Determination of spectral absorption coefficients of particles, dissolved material and phytoplankton for discrete water samples, pp. 125-153. In: Fargion G.S. and Mueller J.L. (eds), Ocean Optics Protocols for Satellite Ocean Color Sensor Validation. NASA/TM-2000-209966.

Mitchell, B.G., M. Kahru, J. Wieland and M. Stramska. 2003. Determination of spectral absorption coefficients of particles, dissolved material and phytoplankton for discrete water samples, pp. 39-64. In: Mueller J.L., G.S. Fargion and C.R. McClain (eds), Ocean Optics Protocols for Satellite Ocean Color Sensor Validation. NASA/TM-2003-211621/Rev4-Vol.IV.

Mueller, J.L., 2003: ``Overview of Measurement and Data Analysis Methods." In: Mueller, J.L., and 17 Coauthors, Ocean Optics Protocols for Satellite Ocean Color Sensor Validation,

Revision 4, Volume III: Radiometric Measurements and Data Analysis Protocols. NASA Tech. Memo. 2003-211621/Rev4-Vol.III, NASA Goddard Space Flight Center, Greenbelt, Maryland, 1-20.

Nelson, J.R. and S. Guarda. 1995. Particulate and dissolved spectral absorption on the continental shelf of the southeastern United States. J. Geophys. Res. 100: 8715-8732.

Nelson, N.B., C.A. Carlson and D.K. Steinberg. 2004. Production of chromophoric dissolved organic matter by Sargasso Sea microbes. Mar. Chem. 89: 273-287.

Nelson, N.B., and D.A. Siegel. 2002. Chromophoric DOM in the open ocean. In: Hansell D.A., Carlson C.A. (eds.), Biogeochemistry of Marine Dissolved Organic Matter, p. 547-578, Academic Press.

O'Reilly, J.E., S. Maritorena, B.G. Mitchell, D.A. Siegel, K.L. Carder, S.A. Garver, M. Kahru, and C. McClain, 1998: Ocean color chlorophyll algorithms for SeaWiFS. J. Geophys. Res., 103, 24,937-24,953.

O'Reilly, J.E., S. Maritorena, M.C. O'Brien, D.A. Siegel, D. Toole, B.G. Mitchell, M. Kahru, F.P. Chavez, P. Strutton, G.F. Cota, S.B. Hooker, C.R. McClain, K.L. Carder, F. M¸ller-Karger, L. Harding, A. Magnuson, D. Phinney, G.F. Moore, J. Aiken, K.R. Arrigo, R. Letelier, M. Culver, 2000: ``Ocean Color Chorophyll a Algorithms for SeaWiFS, OC2, and OC4: Version 4," In: O'Reilly, J.E., and 24 Coauthors, SeaWiFS Postlaunch Calibration and Validation Analyses, Part 3. NASA Tech. Memo. 2000-206892, Vol. 11, S.B. Hooker and E.R. Firestone, Eds., NASA Goddard Space Flight Center,break Greenbelt, Maryland, 9-23.

Rennie, S.E., J.J. Largier and S.J. Lentz. 1999. Observations of a pulsed buoyancy current downstream of Chesapeake Bay. J. Geophys. Res. 104(C8): 18,227-18,240.

Rochelle-Newall, E.J., and T.R. Fisher. 2002. Chromophoric dissolved organic matter and dissolved organic carbon in Chesapeake Bay. Mar. Chem. 77: 23-41.

Russ, M.E., et al. 2007. NASA Technical Memo. In prep.

Sanders, T.M. and R.W. Garvine. 2001. Fresh water delivery to the continental shelf and subsequent mixing: An observational study. J. Geophys. Res. 106(C11): 27,087-27,101.

Schubel, J.R. and D.W. Pritchard. 1986. Responses of upper Chesapeake Bay to variations in discharge of the Susquehanna River. Estuaries 9: 236-249.

Schlünz, B. and R.R. Schneider. 2000. Transport of terrestrial organic carbon to the oceans by rivers: re-estimating flux- and burial rates. Int. J. Earth Sci. 88: 599-606.

Sharp, J.H., C.A. Carlson, E.T. Peltzer, D.M. Castle-Ward, K.B. Savidge and K.R. Rinker. 2002. Final dissolved organic carbon broad community intercalibration and preliminary use of DOC reference materials. Mar. Chem. 77: 239-253.

Siegel, D.A., S. Maritorena, N.B. Nelson, and M.J. Behrenfeld. 2005. Independence and interdependencies among global ocean color properties: Reassessing the bio-optical assumption. J. Geophys. Res. 110, C07011, doi:10.1029/2004JC002527.

Siegel, D.A., S. Maritorena, N.B. Nelson, D.A. Hansell, and M. Lorenzi-Kayser. 2002. Global distribution and dynamics of colored dissolved and detrital organic materials. J. Geophys. Res. 107: 21-1-21-14.

Smith, R.C., and K.S. Baker, 1984: Analysis of ocean optical data. Ocean Optics VII, M. Blizard, Ed., SPIE, 478, 119-126.

Steinberg, D.K., N. Nelson, C.A. Carlson, A.C. Prusak. 2004. Production of chromophoric dissolved organic matter (CDOM) in the open ocean by zooplankton and the colonial cyanobacterium Trichodesmium spp. Mar. Ecol. Prog. Ser. 267: 45-56.

USGS. 2007. http://waterdata.usgs.gov/nwis/.
Van Heukelem, L. and C.S. Thomas. 2001. Computer-assisted high-performance liquid chromatography method development with applications to the isolation and analysis of phytoplankton pigments. J. Chrom. A 910: 31-49.
Verity, P.G., J.E. Bauer, C.N. Flagg, D.J. DeMaster and D.J. Repeta. 2002. The Ocean Margins Program: an interdisciplinary study of carbon sources, transformations, and sinks in a temperate continental margin system. Deep-Sea Research 49: 4273-4295.
Vlahos, P., R.F. Chen and D.J. Repeta. 2002. Dissolved organic carbon in the Middle Atlantic Bight. Deep-Sea Research II 49: 4369-4385.
Vodacek, A., N.V. Blough, M.D. DeGrandpre, E.T. Peltzer, and R.K. Nelson. 1997. Seasonal variation of CDOM and DOC in the Middle Atlantic Bight: Terrestrial inputs and photooxidation. Limnol. Oceanogr. 42: 674-686.
Vodacek, A., F.E. Hoge, R.N. Swift, J.K. Yungel, E.T. Peltzer and N.V. Blough. 1995. The use of in situ and airborne fluorescence measurements to determine UV absorption coefficients and DOC concentrations in surface waters. Limnol. Oceanogr. 40: 411-415.
Williams, P.J. leB. 1995. Evidence for the seasonal accumulation of carbon-rich dissolved organic material, its scale in comparison with changes in particulate material and the consequential effect on net C/N assimilation ratios. Mar. Chem. 51: 17-29.

Figure Captions

Figure 1. Map of the study area within the U.S. Middle Atlantic Bight (MAB). Station locations sampled on (a) 30 March to 1 April 2005, (b) 26-30 July 2005, (c) 9-12 May 2006, and (d) 2-6 July 2006. One-day cruises were conducted in the Chesapeake Bay mouth and plume region (see ellipse in panel a; 4-6 stations per cruise) on 27 May and 3 November 2005 and on 6 September and 28 November 2006. Additional samples were collected along a transect across the Chesapeake Bay mouth (open circles in panel a).

Figure 2. Seasonal relationships of dissolved organic carbon (DOC) and (a) $a_{CDOM}(355)$ (chromophoric dissolved organic matter absorption coefficient at 355 nm) or (b) $a_{CDOM}(412)$ within the MAB and between DOC and (c) $a_{CDOM}(355)$ or (d) $a_{CDOM}(412)$ in the Chesapeake Bay mouth and plume region for the 2004-2006 research cruises. Data shown for Fall_Winter_Spring include measurements from all depths sampled, but only the top 2 depths for the Chesapeake Bay mouth transect (depicted in Fig. 1a). Summer data only include the top 2 depths sampled (surface mixed layer) and exclude the Delaware Bay mouth and plume stations.

Figure 3. CDOM algorithms derived from field observations of $a_{CDOM}(355)$ and remote sensing reflectance (Rrs) band ratios include the (a) one-phase exponential decay models and (b) logarithmic models for multiple Rrs band ratios applicable to SeaWiFS and MODIS satellite sensors. The lines in each panel represent the predicted data from the non-linear and linear regression model curve-fitting routines.

Figure 4. Validation results comparing SeaWiFS observations with field measurements for multiple algorithms within 8 hours and 32 hours of the satellite overpass. Figures show the mean absolute percent difference (APD) with 1 standard deviation for (a) $a_{CDOM}(355)$, (b) $a_{CDOM}(443)$, and (c) DOC and the root mean square error (RMSE) for (d) $a_{CDOM}(355)$, (e) $a_{CDOM}(443)$, and (f) DOC (see text for equations of APD and RMSE). Exp_Rrs(412/555): exponential one-phase decay algorithm for the Rrs(412 nm/555 nm) band ratio, Log_Rrs(490/555): logarithmic algorithm for the Rrs(490 nm/555 nm) band ratio.

Figure 5. Validation results comparing MODIS-Aqua observations with field measurements for multiple algorithms within 8 hours and 32 hours of the satellite overpass. Figures show the mean APD of (a) $a_{CDOM}(355)$, (b) $a_{CDOM}(443)$, and (c) DOC and the RMSE for (d) $a_{CDOM}(355)$, (e) $a_{CDOM}(443)$, and (f) DOC. See Fig. 4 for further details.

Figure 6. Validation match-ups comparing MODIS-Aqua- and SeaWiFS-derived products with field measurements for (a) $a_{CDOM}(355)$, (b) $a_{CDOM}(412)$, and (c) $a_{CDOM}(443)$ within 8 hours of satellite overpass and for (d) $a_{CDOM}(355)$, (e) $a_{CDOM}(412)$, and (f) $a_{CDOM}(443)$, within 32 hours of a satellite overpass. The diagonal solid line within each panel represents the one-to-one line. These statistics within the figure represent the results from the linear regression analysis of the match-up data points. The RMSE is computed as described in the text (equation 2). The statistics above the one-to-one line refer to the MODIS-Aqua analysis, and values below the one-to-one line refer to the SeaWiFS analysis.

Figure 7. Match-ups of the expanded validation dataset comparing MODIS-Aqua- and SeaWiFS-derived products with field measurements for (a) $a_{CDOM}(355)$ and (b) $a_{CDOM}(443)$ within 32 hours of a satellite overpass. The expanded validation dataset includes stations where in situ radiometry measurements were used for algorithm development. Statistics above the one-to-one line refer to MODIS-Aqua analysis, and values below the one-to-one line refer to the SeaWiFS analysis. See Fig. 6 caption for additional details.

Figure 8. Validation match-ups comparing MODIS-Aqua- and SeaWiFS-derived products with field measurements (a) DOC within 8 hours of satellite overpass, (b) DOC within 32 hours of satellite overpass, and (c) DOC within 32 hours of satellite overpass for the expanded dataset. See Fig. 7 for additional details.

Figure 9. Validation comparisons of multiple a_{CDOM} wavelengths for (a) MODIS-Aqua and (b) SeaWiFS and the CDOM spectral slope (S) (c) mean APD, (d) mean APD for expanded validation dataset, (e) one-to-one match-ups, and (f) one-to-one match-ups for the expanded validation dataset.

Figure 10. MODIS-Aqua derived satellite images of $a_{CDOM}(355)$ (m^{-1}) for (a) 18 March 2005, (b) 27 May 2005, (c) 5 August 2005, (d) 3 November 2005, (e) 24 December 2005, (f) 15 February 2006, (g) 12 May 2006, and (h) 30 June 2006.

Figure 11. Daily streamflow discharge from the Susquehanna River (Conowingo Dam, head of Chesapeake Bay) and Delaware River (Trenton, NJ) and monthly freshwater outflow from the Chesapeake Bay mouth. The Susquehanna River contributes >50% of the freshwater discharge into Chesapeake Bay. Data sources: http://waterdata.usgs.gov/nwis/; written communication from Gary Fisher, U.S. Geological Survey July 17, 2007.

Figure 12. SeaWiFS derived satellite images of DOC (μmol C L^{-1}) for (a) 5 April 2005, (b) 27 May 2005, (c) 5 August 2005, (d) 3 November 2005, (e) 16 February 2006, (f) 12 May 2006, (g) 30 June 2006, and (h) 26 November, 2006.

Figure 13. Seasonal and interannual comparisons of DOC for discrete MODIS images from (a) 2005 and (b) 2006 and (c) field measurements.

Table 1. Validated satellite a_{CDOM} algorithms derived from field observations of $a_{CDOM}(\lambda)$ and remote sensing reflectance (Rrs) band ratios. The form of the algorithm is the nonlinear one-phase exponential decay regression model: Rrs ratio = $a \bullet e^{-c \bullet a_{CDOM}(355)} + b$. The non-linear function was solved for a_{CDOM} yielding the following equation: $a_{CDOM}(\lambda) = \ln((\text{Rrs ratio} - a)/b)/(-c)$. The Rrs(490 nm/551 nm) band ratio algorithms were applied to derive a_{CDOM} from MODIS-Aqua, and no adjustments were made to field-derived Rrs at 490 nm to match the 488 nm MODIS-Aqua band.

Product	Rrs Band Ratio	a	b	c	N	RMSE[a] (Rrs ratio)	R^2
$a_{CDOM}(355)$	490/555	0.4847	3.055	3.642	34	0.1496	0.908
	490/551	0.4934	2.731	3.512	34	0.1377	0.907
$a_{CDOM}(412)$	490/555	0.4443	2.599	8.327	34	0.1354	0.925
	490/551	0.4553	2.345	8.045	34	0.1244	0.924
$a_{CDOM}(443)$	490/555	0.4247	2.453	13.586	34	0.1482	0.910
	490/551	0.4363	2.221	13.126	34	0.1355	0.910

[a] RMSE – Root Mean Square Error represents the standard deviation of the residuals for the Rrs band ratios from the non-linear regression analysis.

Table 2. DOC algorithms derived from model II linear regression analysis of DOC and $a_{CDOM}(355)$ field measurements. The Chesapeake Bay mouth and plume equations represent a subset of the MAB dataset. Data were transformed to meet normality assumptions of linear regression analysis. The equation takes the following form: $DOC = 1/(\ln(a_{CDOM}(355)) \bullet (-m) + b)$. The $a_{CDOM}(355)$ algorithms shown in Table 2 can be entered into this equation to obtain DOC directly from satellite Rrs products.

Season	Region	m	b	N	RMSE[a]	R^2	p
Fall-Winter-Spring	MAB	0.0047465	0.0075058	277	0.000618	0.954	<0.0001
	Chesapeake Bay mouth and plume	0.0046740	0.0073888	148	0.000517	0.938	<0.0001
Summer	MAB	0.0030323	0.0061522	160	0.000684	0.874	<0.0001
	Chesapeake Bay mouth and plume	0.0034165	0.0060366	87	0.000519	0.813	<0.0001

[a] RMSE – Root Mean Square Error refers to DOC in transformed units (1/DOC).

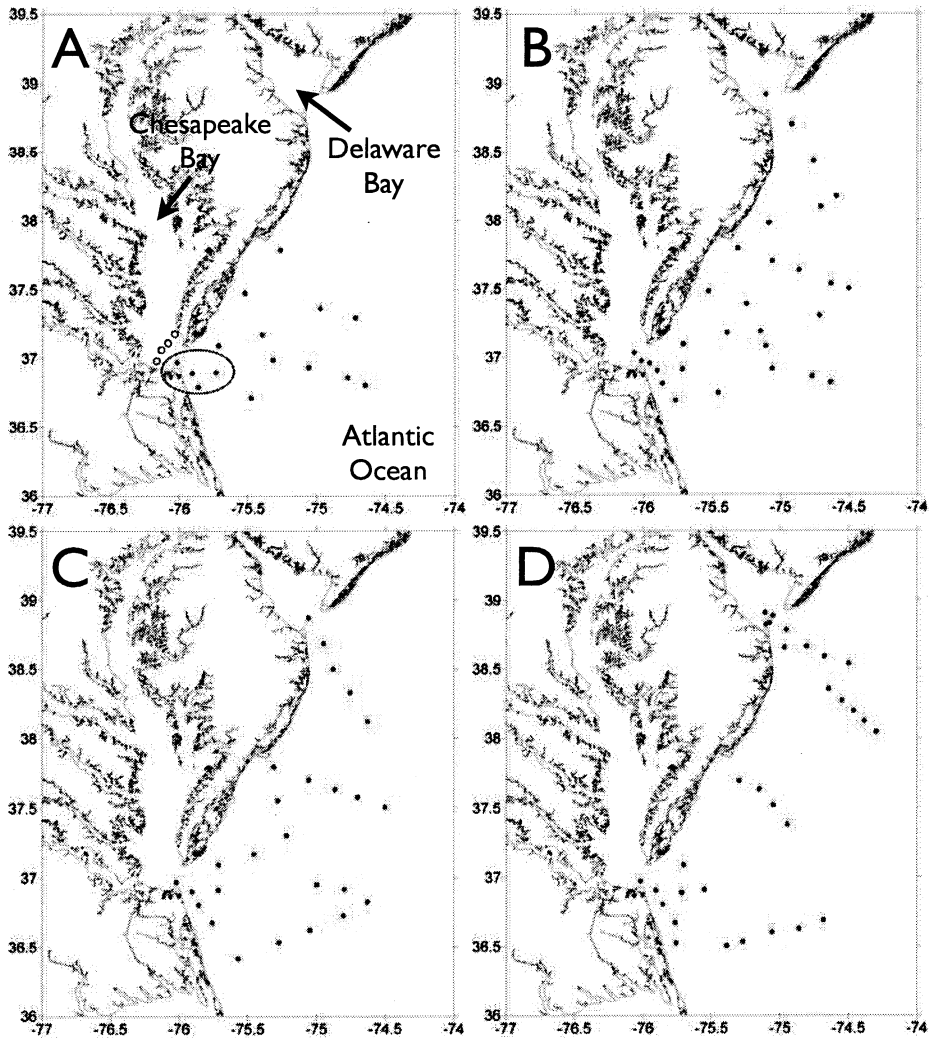
A
B
C
D
Chesapeake Bay
Delaware Bay
Atlantic Ocean
39.5
39
38.5
38
37.5
37
36.5
36
-77
-76.5
-76
-75.5
-75
-74.5
-74

Figure 1

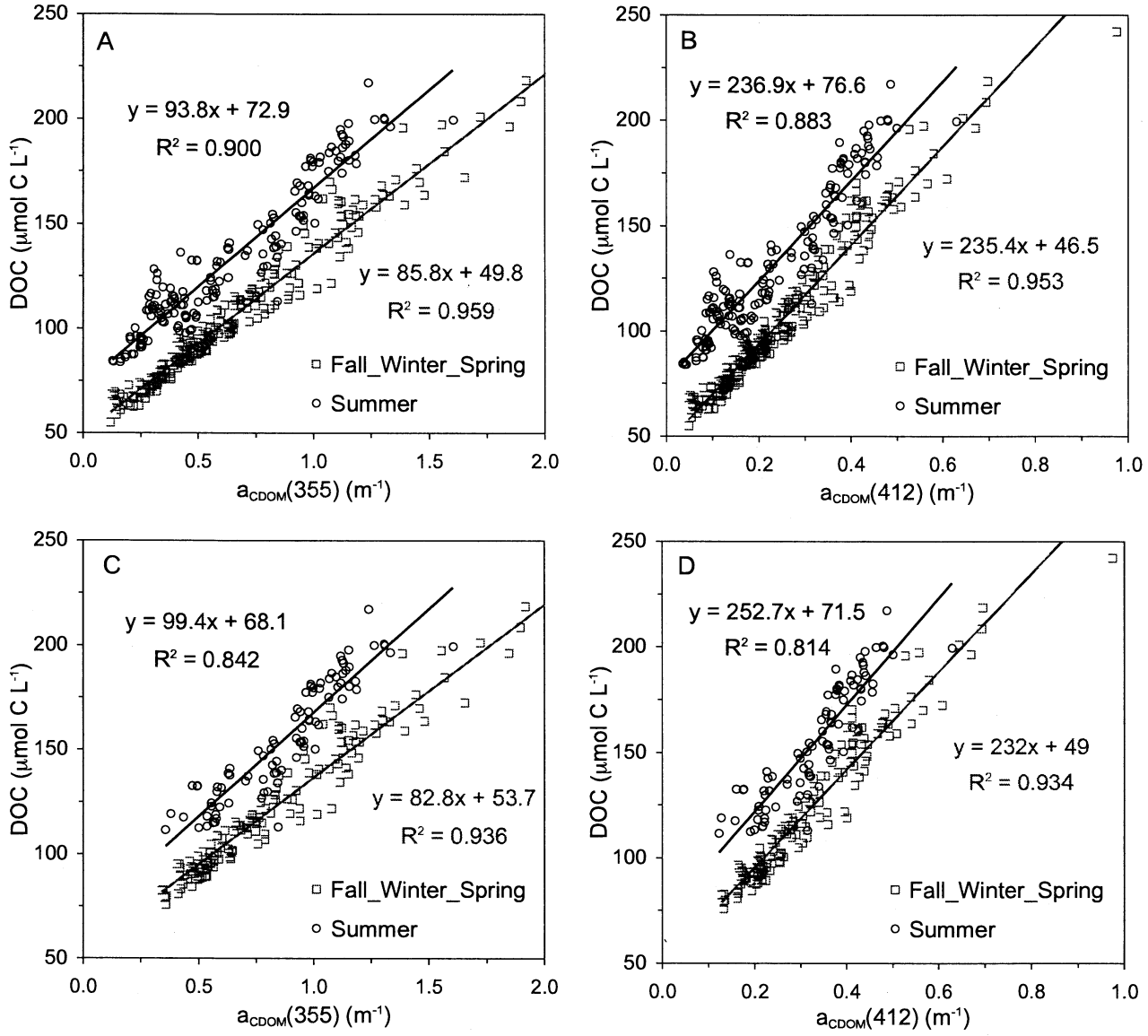
A
y = 93.8x + 72.9
R² = 0.900
y = 85.8x + 49.8
R² = 0.959
Fall_Winter_Spring
Summer
DOC (µmol C L⁻¹)
a_CDOM(355) (m⁻¹)
B
y = 236.9x + 76.6
R² = 0.883
y = 235.4x + 46.5
R² = 0.953
Fall_Winter_Spring
Summer
DOC (µmol C L⁻¹)
a_CDOM(412) (m⁻¹)
C
y = 99.4x + 68.1
R² = 0.842
y = 82.8x + 53.7
R² = 0.936
Fall_Winter_Spring
Summer
DOC (µmol C L⁻¹)
a_CDOM(355) (m⁻¹)
D
y = 252.7x + 71.5
R² = 0.814
y = 232x + 49
R² = 0.934
Fall_Winter_Spring
Summer
DOC (µmol C L⁻¹)
a_CDOM(412) (m⁻¹)

Figure 2

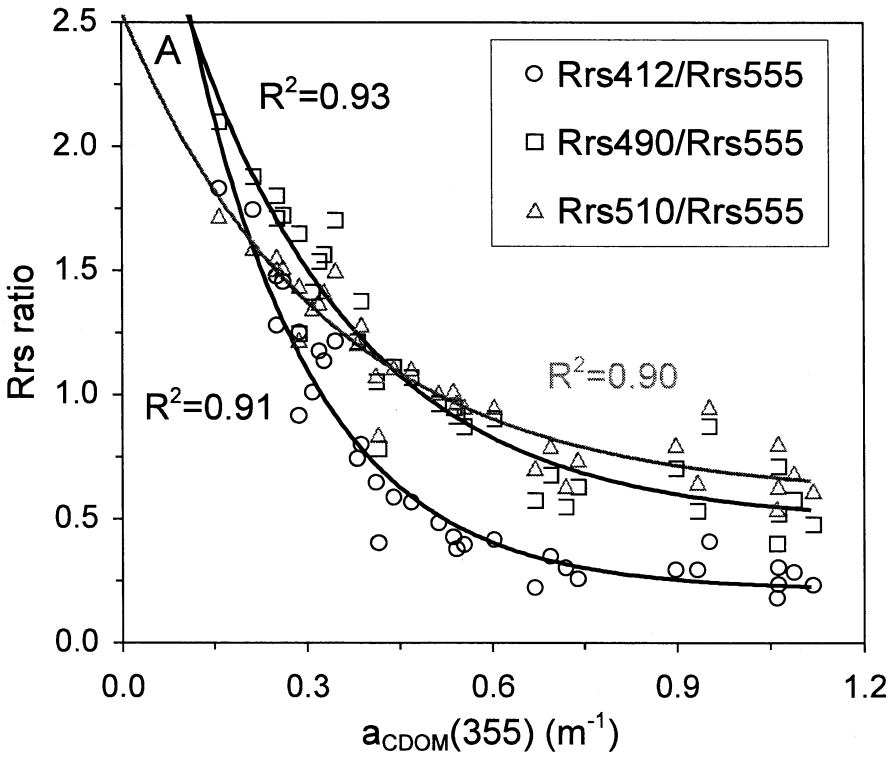
A
R^2=0.93
R^2=0.90
R^2=0.91
Rrs412/Rrs555
Rrs490/Rrs555
Rrs510/Rrs555
Rrs ratio
2.5
2.0
1.5
1.0
0.5
0.0
0.0
0.3
0.6
0.9
1.2
$a_{CDOM}(355)$ (m^{-1})

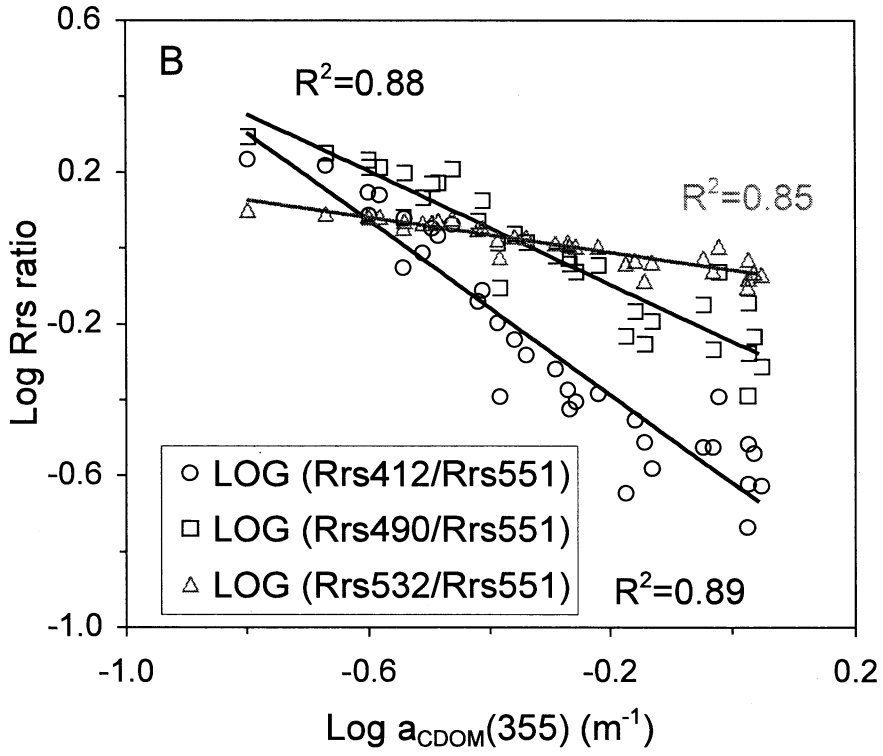
B
R^2=0.88
R^2=0.85
R^2=0.89
LOG (Rrs412/Rrs551)
LOG (Rrs490/Rrs551)
LOG (Rrs532/Rrs551)
Log Rrs ratio
0.6
0.2
-0.2
-0.6
-1.0
-1.0
-0.6
-0.2
0.2
Log $a_{CDOM}(355)$ (m^{-1})

Figure 3

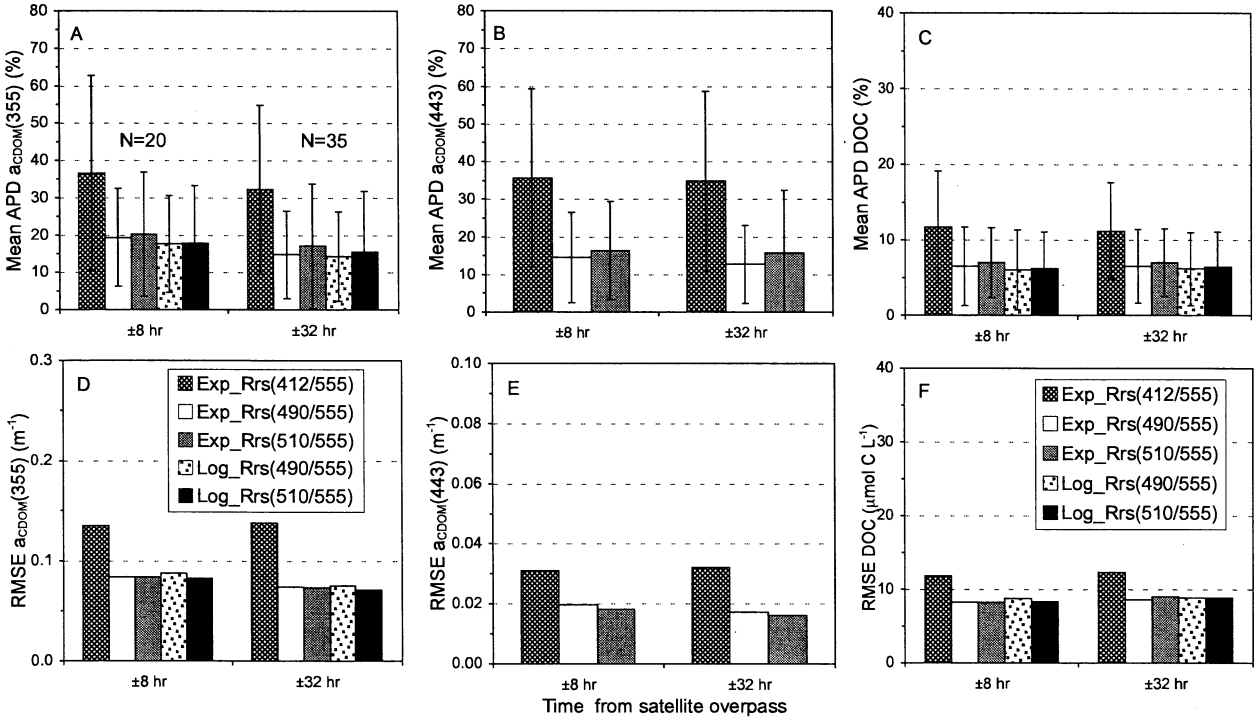
A
B
C
D
E
F
N=20
N=35
Mean APD $a_{CDOM}(355)$ (%)
Mean APD $a_{CDOM}(443)$ (%)
Mean APD DOC (%)
RMSE $a_{CDOM}(355)$ (m^{-1})
RMSE $a_{CDOM}(443)$ (m^{-1})
RMSE DOC_s (µmol C L^{-1})
±8 hr
±32 hr
Exp_Rrs(412/555)
Exp_Rrs(490/555)
Exp_Rrs(510/555)
Log_Rrs(490/555)
Log_Rrs(510/555)
Time from satellite overpass

Figure 4

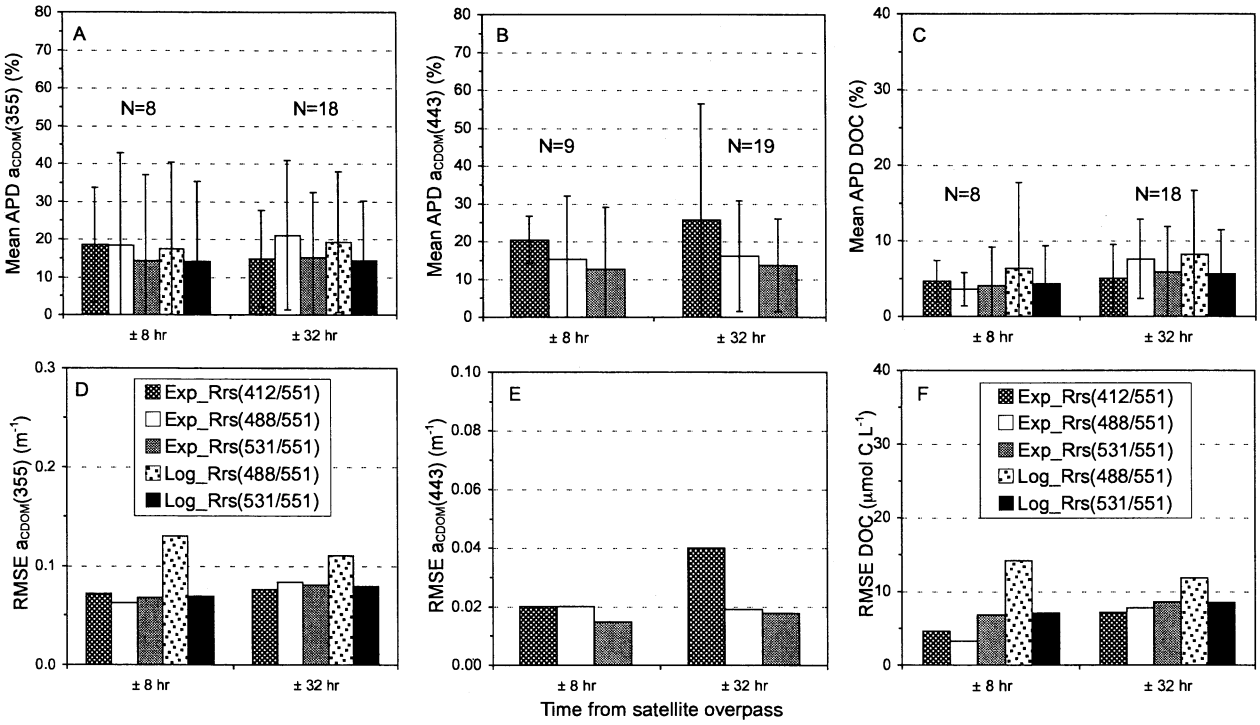
A
N=8
N=18
Mean APD $a_{CDOM}(355)$ (%)
± 8 hr
± 32 hr
B
N=9
N=19
Mean APD $a_{CDOM}(443)$ (%)
C
N=8
N=18
Mean APD DOC (%)
D
Exp_Rrs(412/551)
Exp_Rrs(488/551)
Exp_Rrs(531/551)
Log_Rrs(488/551)
Log_Rrs(531/551)
RMSE $a_{CDOM}(355)$ (m^{-1})
E
RMSE $a_{CDOM}(443)$ (m^{-1})
F
RMSE DOC_s (µmol $C_s L^{-1}$)
Time from satellite overpass

Figure 5

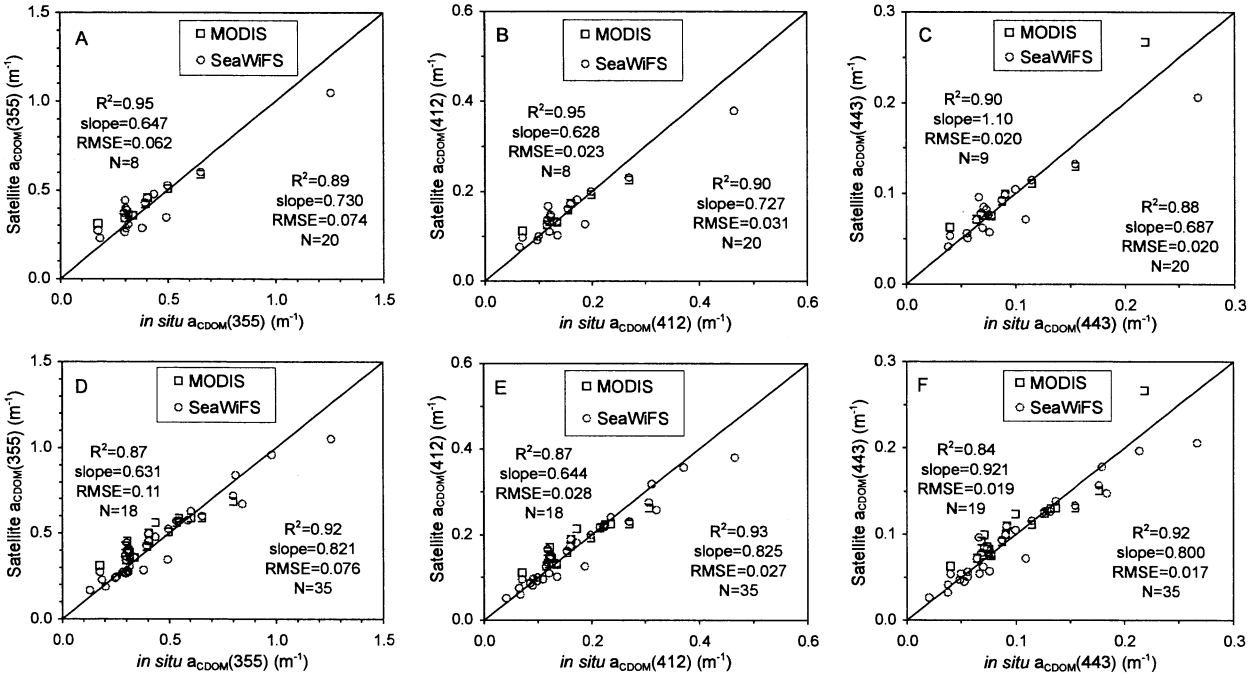
A
MODIS
SeaWiFS
R²=0.95
slope=0.647
RMSE=0.062
N=8
R²=0.89
slope=0.730
RMSE=0.074
N=20
Satellite a_CDOM(355) (m⁻¹)
in situ a_CDOM(355) (m⁻¹)
B
MODIS
SeaWiFS
R²=0.95
slope=0.628
RMSE=0.023
N=8
R²=0.90
slope=0.727
RMSE=0.031
N=20
Satellite a_CDOM(412) (m⁻¹)
in situ a_CDOM(412) (m⁻¹)
C
MODIS
SeaWiFS
R²=0.90
slope=1.10
RMSE=0.020
N=9
R²=0.88
slope=0.687
RMSE=0.020
N=20
Satellite a_CDOM(443) (m⁻¹)
in situ a_CDOM(443) (m⁻¹)
D
MODIS
SeaWiFS
R²=0.87
slope=0.631
RMSE=0.11
N=18
R²=0.92
slope=0.821
RMSE=0.076
N=35
Satellite a_CDOM(355) (m⁻¹)
in situ a_CDOM(355) (m⁻¹)
E
MODIS
SeaWiFS
R²=0.87
slope=0.644
RMSE=0.028
N=18
R²=0.93
slope=0.825
RMSE=0.027
N=35
Satellite a_CDOM(412) (m⁻¹)
in situ a_CDOM(412) (m⁻¹)
F
MODIS
SeaWiFS
R²=0.84
slope=0.921
RMSE=0.019
N=19
R²=0.92
slope=0.800
RMSE=0.017
N=35
Satellite a_CDOM(443) (m⁻¹)
in situ a_CDOM(443) (m⁻¹)

Figure 6

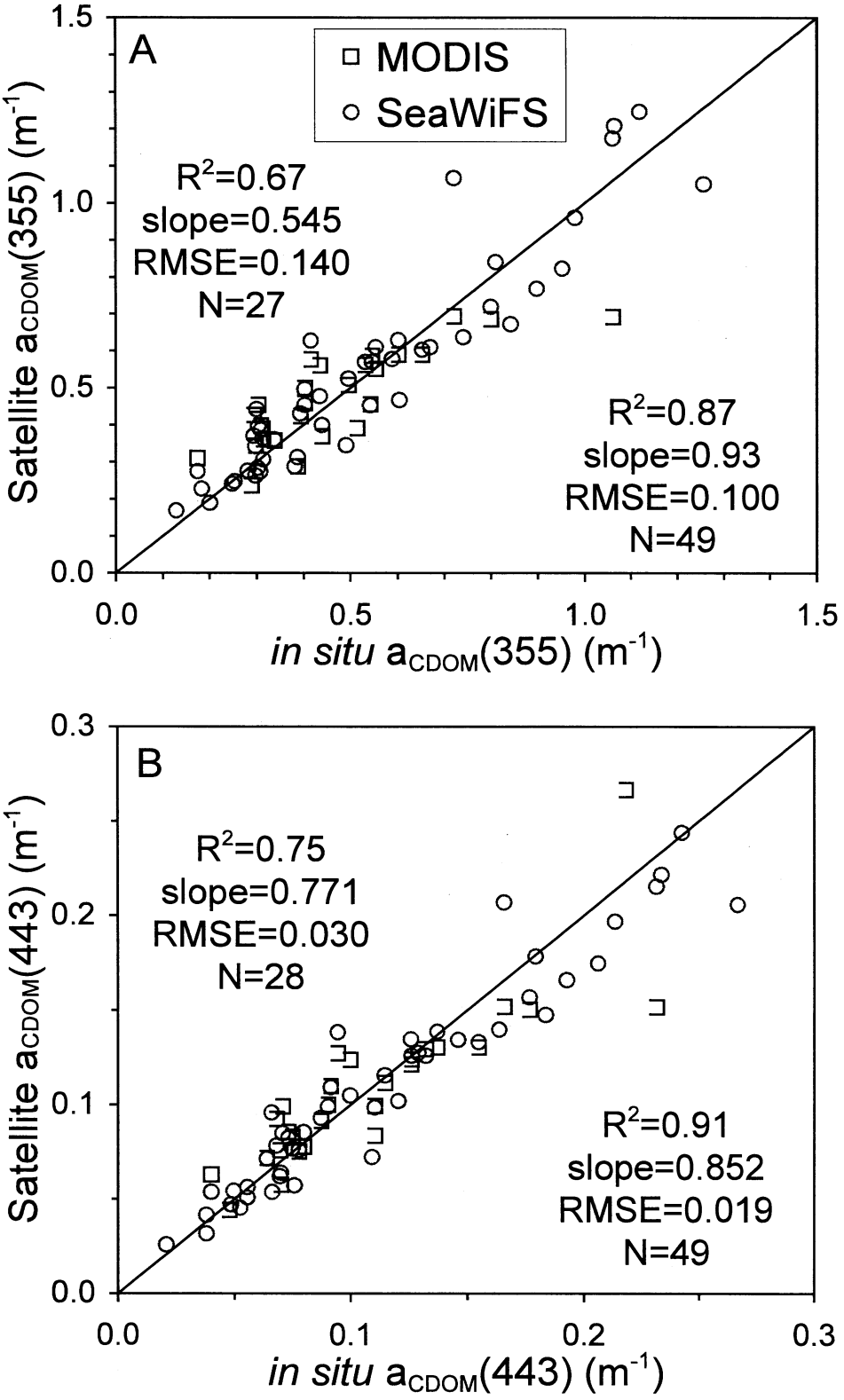
A
MODIS
SeaWiFS
R²=0.67
slope=0.545
RMSE=0.140
N=27
R²=0.87
slope=0.93
RMSE=0.100
N=49
Satellite a_CDOM(355) (m⁻¹)
in situ a_CDOM(355) (m⁻¹)
0.0
0.5
1.0
1.5
B
R²=0.75
slope=0.771
RMSE=0.030
N=28
R²=0.91
slope=0.852
RMSE=0.019
N=49
Satellite a_CDOM(443) (m⁻¹)
in situ a_CDOM(443) (m⁻¹)
0.0
0.1
0.2
0.3

Figure 7

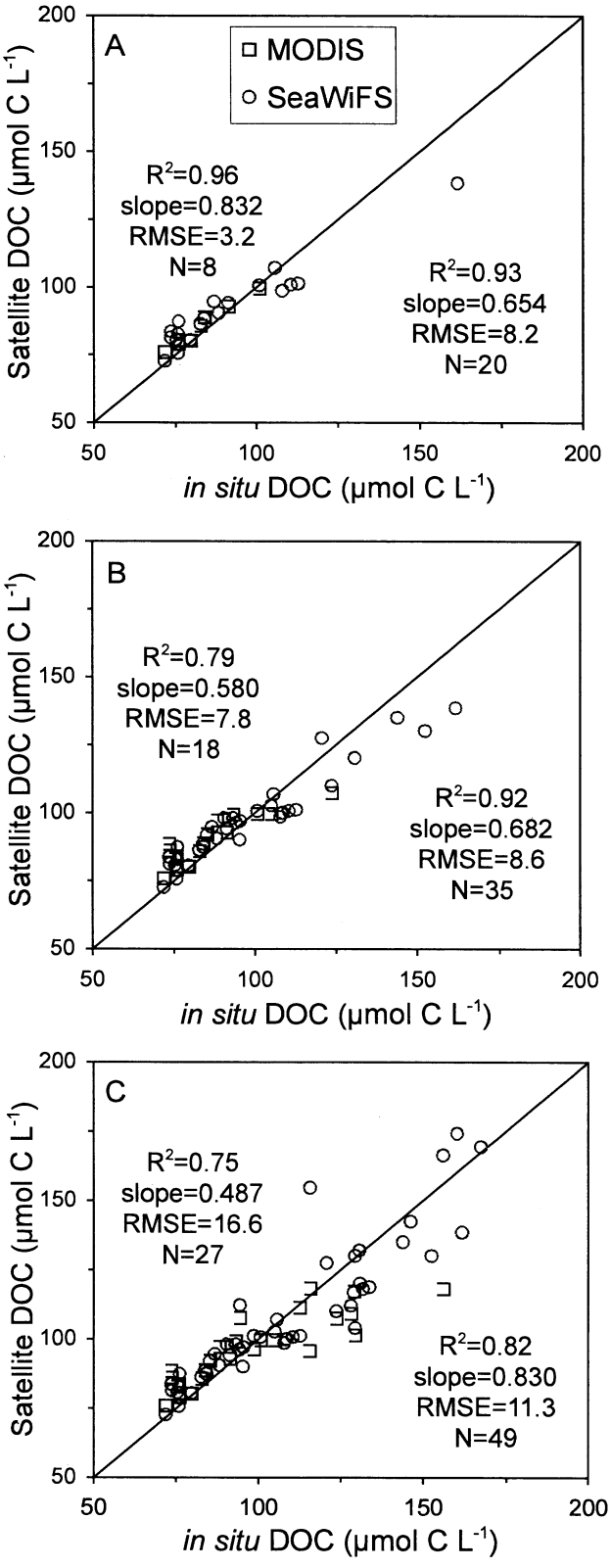
A
MODIS
SeaWiFS
R²=0.96
slope=0.832
RMSE=3.2
N=8
R²=0.93
slope=0.654
RMSE=8.2
N=20
B
R²=0.79
slope=0.580
RMSE=7.8
N=18
R²=0.92
slope=0.682
RMSE=8.6
N=35
C
R²=0.75
slope=0.487
RMSE=16.6
N=27
R²=0.82
slope=0.830
RMSE=11.3
N=49
Satellite DOC (µmol C L⁻¹)
in situ DOC (µmol C L⁻¹)
50
100
150
200

Figure 8

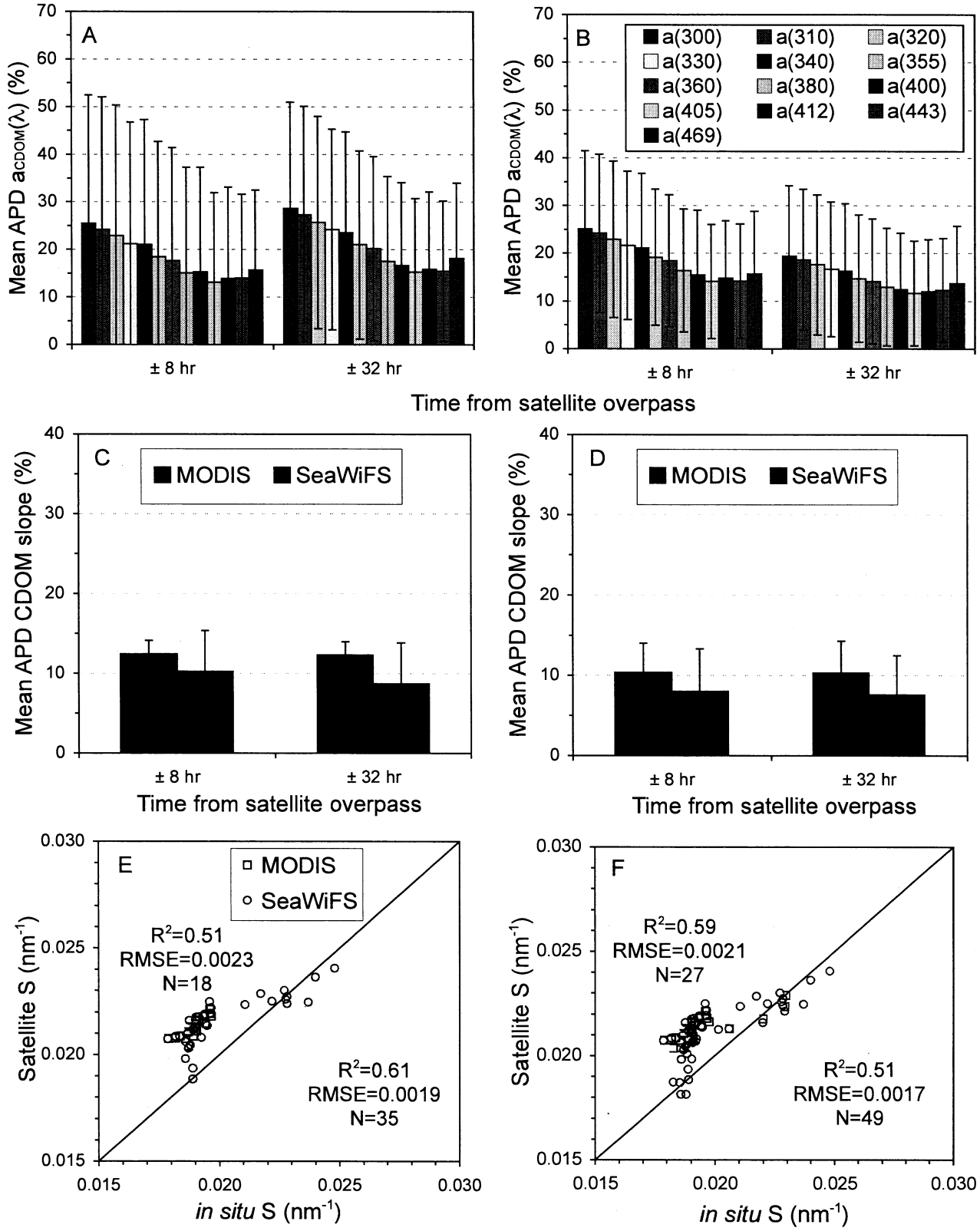
A
B
Mean APD aCDOM(λ) (%)
a(300)
a(310)
a(320)
a(330)
a(340)
a(355)
a(360)
a(380)
a(400)
a(405)
a(412)
a(443)
a(469)
± 8 hr
± 32 hr
Time from satellite overpass
C
D
MODIS
SeaWiFS
Mean APD CDOM slope (%)
E
F
Satellite S (nm-1)
in situ S (nm-1)
R2=0.51
RMSE=0.0023
N=18
R2=0.61
RMSE=0.0019
N=35
R2=0.59
RMSE=0.0021
N=27
R2=0.51
RMSE=0.0017
N=49

Figure 9

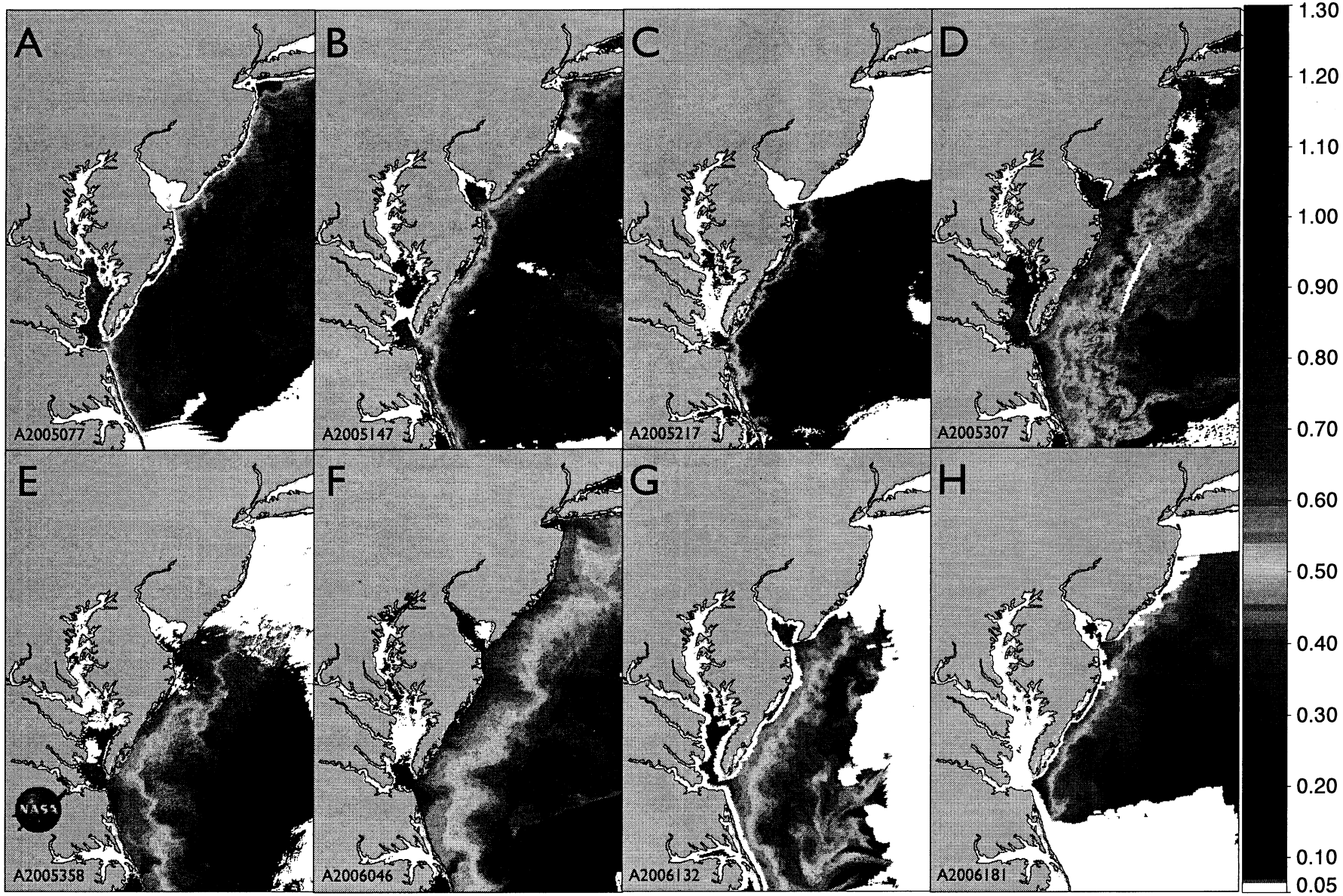
A
B
C
D
E
F
G
H
A2005077
A2005147
A2005217
A2005307
A2005358
A2006046
A2006132
A2006181
NASA
1.30
1.20
1.10
1.00
0.90
0.80
0.70
0.60
0.50
0.40
0.30
0.20
0.10
0.05

Figure 10

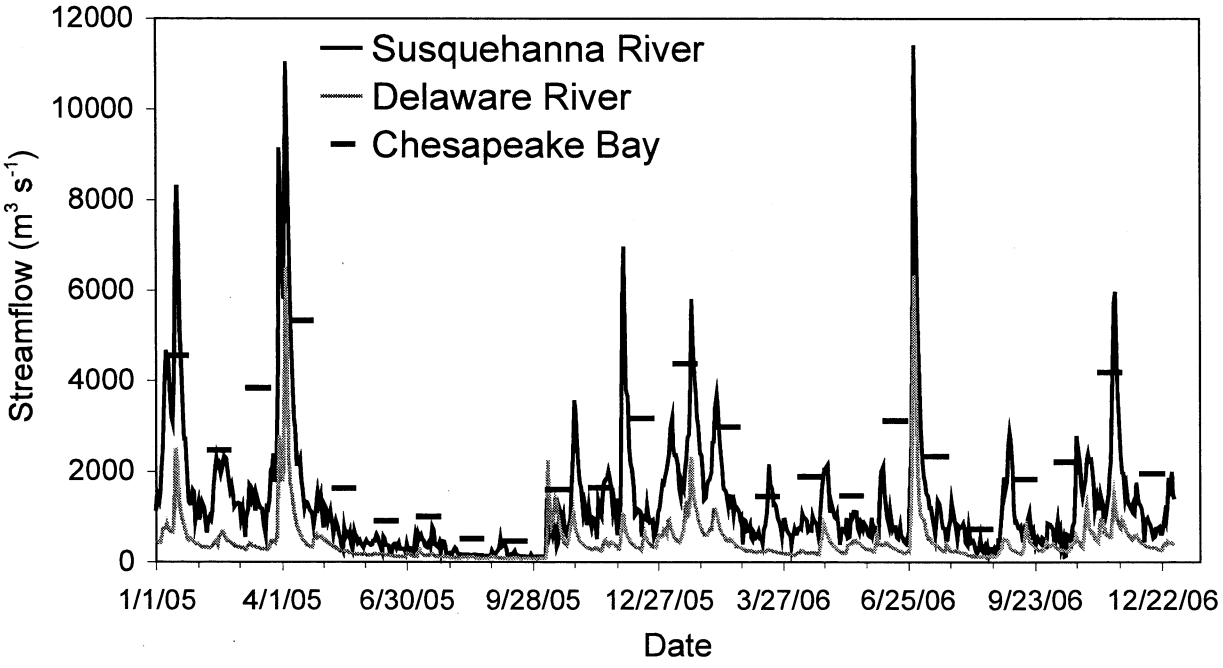
12000
10000
8000
6000
4000
2000
0
Streamflow ($m^3 s^{-1}$)
Susquehanna River
Delaware River
Chesapeake Bay
1/1/05
4/1/05
6/30/05
9/28/05
12/27/05
3/27/06
6/25/06
9/23/06
12/22/06
Date

Figure 11

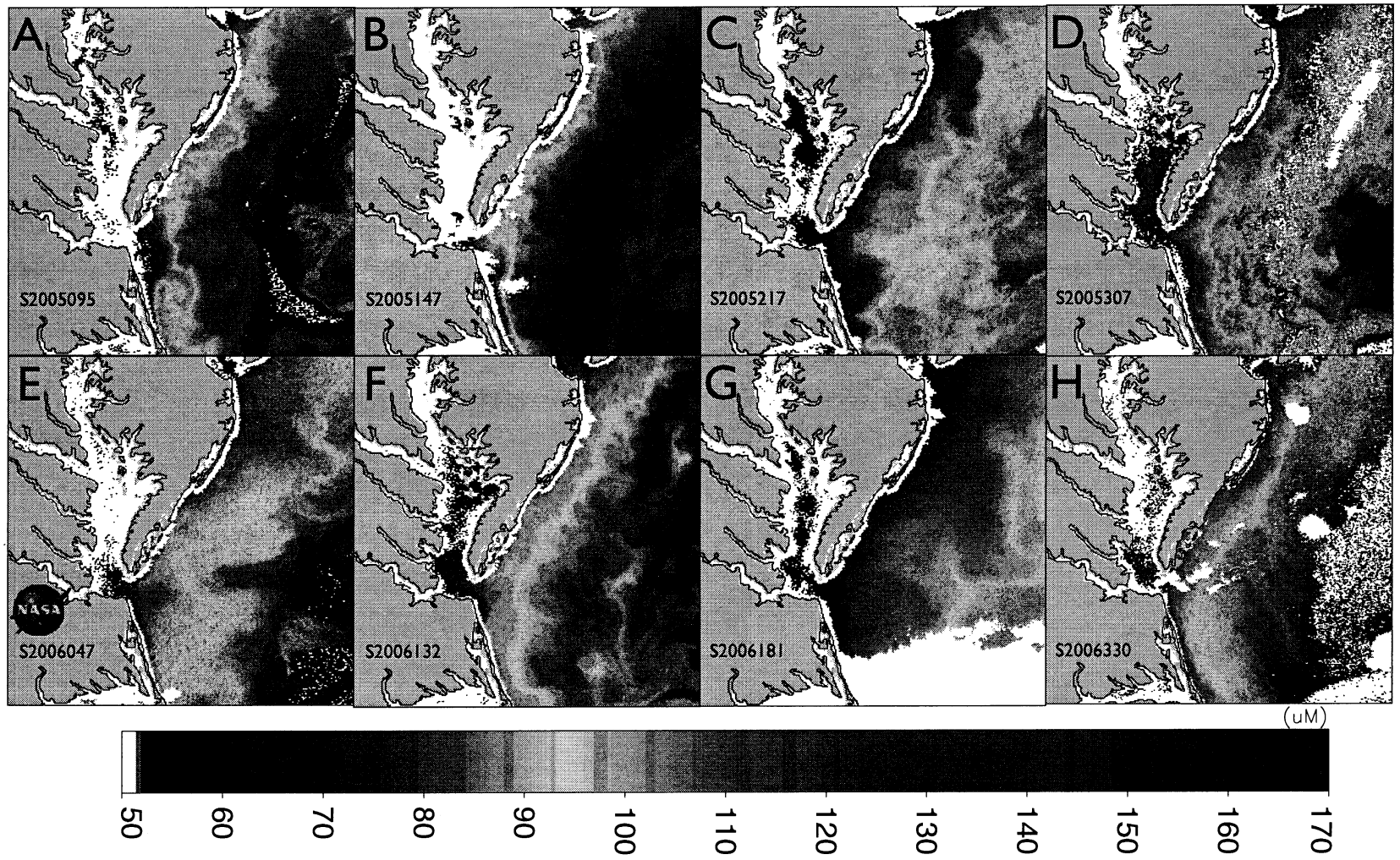
A
S2005095
B
S2005147
C
S2005217
D
S2005307
E
S2006047
F
S2006132
G
S2006181
H
S2006330
(uM)
50
60
70
80
90
100
110
120
130
140
150
160
170

Figure 12

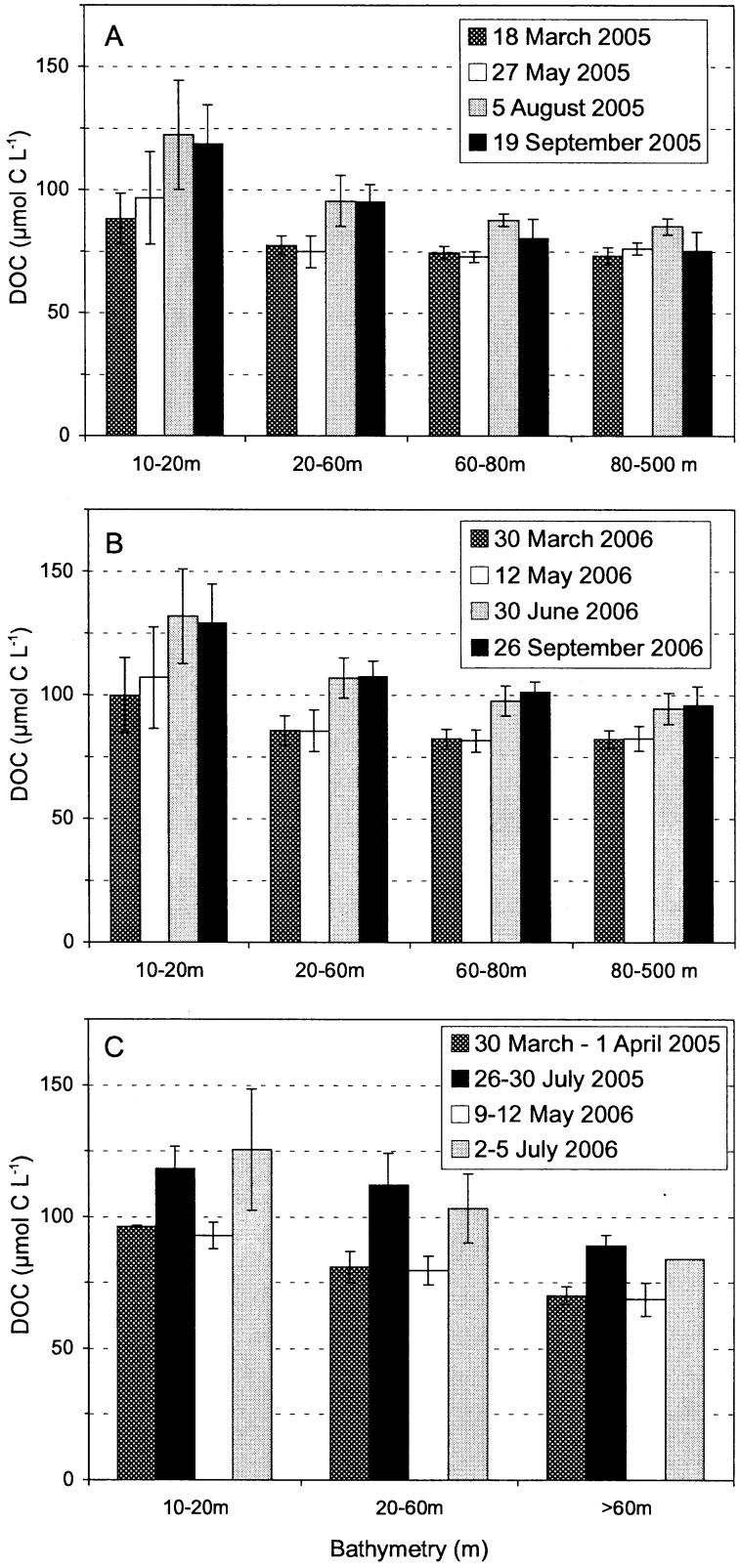
A
18 March 2005
27 May 2005
5 August 2005
19 September 2005
DOC (µmol C L-1)
150
100
50
0
10-20m
20-60m
60-80m
80-500 m
B
30 March 2006
12 May 2006
30 June 2006
26 September 2006
DOC (µmol C L-1)
150
100
50
0
10-20m
20-60m
60-80m
80-500 m
C
30 March - 1 April 2005
26-30 July 2005
9-12 May 2006
2-5 July 2006
DOC (µmol C L-1)
150
100
50
0
10-20m
20-60m
>60m
Bathymetry (m)

Figure 13